Cell

Structural and Biochemical Studies of ALIX/AIP1 and Its Role in Retrovirus Budding

Robert D. Fisher,[1,3] Hyo-Young Chung,[1,3] Qianting Zhai,[1] Howard Robinson,[2] Wesley I. Sundquist,[1,*] and Christopher P. Hill[1,*]
[1] Department of Biochemistry, University of Utah School of Medicine, Salt Lake City, UT 84112, USA
[2] Department of Biology, Brookhaven National Laboratory, Upton, NY 11973, USA
[3] These authors contributed equally to this work.
*Correspondence: wes@biochem.utah.edu (W.I.S.), chris@biochem.utah.edu (C.P.H.)
DOI 10.1016/j.cell.2007.01.035

SUMMARY

ALIX/AIP1 functions in enveloped virus budding, endosomal protein sorting, and many other cellular processes. Retroviruses, including HIV-1, SIV, and EIAV, bind and recruit ALIX through YPX_nL late-domain motifs (X = any residue; n = 1–3). Crystal structures reveal that human ALIX is composed of an N-terminal Bro1 domain and a central domain that is composed of two extended three-helix bundles that form elongated arms that fold back into a "V." The structures also reveal conformational flexibility in the arms that suggests that the V domain may act as a flexible hinge in response to ligand binding. YPX_nL late domains bind in a conserved hydrophobic pocket on the second arm near the apex of the V, whereas CHMP4/ESCRT-III proteins bind a conserved hydrophobic patch on the Bro1 domain, and both interactions are required for virus budding. ALIX therefore serves as a flexible, extended scaffold that connects retroviral Gag proteins to ESCRT-III and other cellular-budding machinery.

INTRODUCTION

Many enveloped RNA viruses use short peptide motifs, termed "late domains," to recruit cellular factors that facilitate budding (reviewed in Bieniasz, 2006; Demirov and Freed, 2004; Morita and Sundquist, 2004). Two of the best characterized late domains are the PTAP motif, which binds and recruits TSG101 (*t*umor *s*usceptibility *g*ene 101; Demirov et al., 2002; Garrus et al., 2001; Gottlinger et al., 1991; Huang et al., 1995; Martin-Serrano et al., 2001; VerPlank et al., 2001), and the YPX_nL motif (where X can vary in sequence and length), which binds ALIX/AIP1 (*AL*G-2-*i*nteracting protein *X*; Chen et al., 2005; Puffer et al., 1997; Strack et al., 2003; Vincent et al., 2003). YPX_nL late domains can vary in sequence and can function alone or together with PTAP late domains. For example, the structural $p6^{Gag}$ protein of HIV-1_{NL4-3} contains $_{7}PTAP_{10}$ and $_{36}YPLASL_{41}$ late domains that function in tandem, whereas the analogous EIAV $p9^{Gag}$ protein contains a single $_{23}YPDL_{26}$ late domain. In principle, multiple late domains could synergistically enhance virus release and/or expand viral tropism.

Both TSG101 (Vps23p in yeast) and ALIX (Bro1p) help sort membrane proteins into vesicles that bud into the lumen of multivesicular bodies (MVB), which supports the idea that virus budding and MVB vesicle formation are highly related processes. The requirements for MVB protein sorting and vesicle formation are best understood in yeast, where the process requires the action of at least 18 different "Class E" proteins. Most, but not all, Class E proteins are stable subunits of the three ESCRT complexes (*e*ndosomal *s*orting *c*omplexes *r*equired for *t*ransport; Hurley and Emr, 2006). Humans have at least one homolog of every yeast Class E protein, and MVB vesicle sorting therefore appears to be a highly conserved process, albeit one that occurs with considerably greater complexity in mammals.

TSG101 functions as the central subunit of ESCRT-I, which recognizes ubiquitylated membrane-protein cargoes and helps recruit the downstream machinery necessary for protein sorting and MVB vesicle formation (Hurley and Emr, 2006). This downstream machinery includes the ESCRT-III and VPS4-LIP5 complexes, which appear to be intimately involved in the actual mechanics of protein sorting and vesicle formation. ALIX is also a Class E protein and can interact directly with both ESCRT-I and ESCRT-III but is not a stable subunit of either complex (reviewed in Odorizzi, 2006). The yeast homolog Bro1p also recruits the deubiquitylating enzyme Doa4p, which removes ubiquitin from cargoes as they are sorted into MVB vesicles (Dejournett et al., 2006; Luhtala and Odorizzi, 2004).

In addition to its roles in virus budding and MVB cargo sorting, ALIX has also been implicated in a number of other important cellular processes, including (1) MVB vesicle fission and back fusion via regulation of the conical lipid,

lysobisphosphatidic acid (LBPA; reviewed in van der Goot and Gruenberg, 2006); (2) endocytosis via interactions with the membrane-curvature-sensing endophilins (Chatellard-Causse et al., 2002; Gallop and McMahon, 2005); (3) cell-surface-receptor downregulation via direct interactions with cell-surface receptors (Geminard et al., 2004) and through antagonism of the Cbl-SETA/CIN85-endophilin complex (Schmidt et al., 2004); (4) spatial distribution of endosomes via regulation of cortical actin (Cabezas et al., 2005); (5) cell motility/adhesion via interactions with FAK (*f*ocal *a*dhesion *k*inase), PYK2 (*p*roline-rich *t*yrosine *k*inase *2*; Schmidt et al., 2003), and possibly also RabGAPLP (*Rab G*TPase-*a*ctivating *p*rotein-*l*ike *p*rotein; Ichioka et al., 2005); (6) apoptosis via interactions with the calcium-binding EF-hand protein ALG-2 (*a*poptosis-*l*inked *g*ene-2; reviewed in Sadoul, 2006); (7) regulation of the JNK signaling pathway via interactions with ALG-2 and the ubiquitin E3 ligase POSH (*p*lenty *o*f *SH*3 domains; Tsuda et al., 2006). The latter observation is of particular interest because POSH is also required for HIV-1 release (Alroy et al., 2005), which raises the possibility that the ALIX-POSH-ALG-2 complex could function in HIV-1 budding.

In summary, it is now apparent that ALIX performs a series of important functions in the endosomal pathway, in cytoskeletal dynamics, and in enveloped virus budding. However, the mechanistic bases for these seemingly diverse ALIX functions are not known. Our studies were therefore undertaken with the goals of elucidating the structure of ALIX, determining how it interacts with retroviral Gag proteins, and testing its requirements for functioning in virus budding.

RESULTS

Structural Studies of Human ALIX

As illustrated in Figure 1A, human ALIX can be subdivided into three regions; the Bro1 domain (residues 1–358), the "V" domain (362–702), and the proline-rich region (PRR; 703–868). Constructs containing the PRR did not express well in *E. coli*, but constructs spanning the Bro1 and V domains could be expressed and purified. A series of $ALIX_{Bro1\text{-}V}$ proteins with loop mutations were surveyed to identify a protein that would crystallize. The $KK_{268,269}YY$ mutation enabled crystallization (apparently because Tyr268 makes an important crystal contact), and the structure of this protein (hereafter termed $ALIX_{Bro1\text{-}V}$) was determined at a resolution of 3.3 Å (R_{free} = 31.7%; Figures 1B and S1; Table S1). Isolated wild-type Bro1 and V domains were also crystallized and their structures were determined at higher resolutions (2.55 Å, R_{free} = 27.4% and 2.6 Å, R_{free} = 30.2%, respectively; see Figures 1C–1E). The V-domain crystals contained two molecules in the asymmetric unit, and the different structures therefore provided three independent views of the ALIX V domain.

Global Architecture of $ALIX_{Bro1\text{-}V}$

As illustrated in Figure 1B, the $ALIX_{Bro1\text{-}V}$ protein adopts an extended conformation in which the Bro1 and V domains form discrete elements. Like its yeast analog, Bro1p (Kim et al., 2005), $ALIX_{Bro1}$ is shaped like a banana, with a long dimension of ~100 Å. The domain is organized about a core tetratricopeptide repeat (TPR) composed of three helical hairpins that associate into a right-handed superhelix (Figure 1C). The ALIX V domain is composed of two extended arms that fold back on themselves at an angle of ~30° to form a V. The arms are 77 Å (arm1) and 90 Å (arm2) in length, and each is organized about an extended three-helix bundle (Figures 1D and 1E). The V-shaped conformation brings the N-terminal Bro1 domain and the C-terminal PRR (not present in the structure) into spatial proximity, thereby explaining how Src kinase can simultaneously dock to the Bro1 domain and phosphorylate Tyr residues in the ALIX C-terminal tail (Schmidt et al., 2005).

$ALIX_{Bro1\text{-}V}$ has a highly asymmetric shape because the long axes of the Bro1 and arm1 elements connect in parallel. As a result, $ALIX_{Bro1\text{-}V}$ is ~150 Å in its longest dimension but less than 50 Å in its other two. Small-angle X-ray scattering profiles fit the crystal model well (R.D.F. and H. Tsuruta, unpublished data), which indicates that the crystal structure provides a good model for the solution structure of the uncomplexed protein. Nevertheless, we speculate that the different domains could change their relative orientations in response to environmental cues like ligand binding because the Bro1 and V domains are connected by a single tripeptide linker ($_{359}VPV_{361}$) that makes only limited noncovalent contacts (Figures 1B and 2A). Moreover, the V-domain arm trajectories vary in the three different structures, which results in relative displacements of up to 10 Å at their tips (Figure 2B). Finally, the loop region between the two arms of the V domain also has the potential to act as a hinge (Figure 2C and Discussion). Thus, the overall impression is that $ALIX_{Bro1\text{-}V}$ is a scaffold composed of extended domains that may reorient in response to ligand binding.

Structure of the Bro1 Domain

The three helical hairpins that comprise the $ALIX_{Bro1}$ TPR core (α4/5, α6/7, and α8/9) are each ~50 residues in length. They form a right-handed solenoid with a rotation of ~20° between each helical pair. The core is flanked on one side by α10 (left in Figure 1C) and on the other by a small β sheet (β1, β2) and a three-helix bundle (α1–3). Both the N and C termini adopt extended conformations that traverse opposite sides of the domain, with the first 17 residues extending along the convex surface and the final 43 residues extending across the concave surface.

As expected, human $ALIX_{Bro1}$ generally resembles its yeast counterpart (Kim et al., 2005), with an overall rmsd of 2.8 Å over 338 equivalent Cα positions (Figure S2). The character of the domain surface is also largely conserved, with two exposed hydrophobic patches centered about Tyr319 and Phe199. The first patch forms the docking site for Src kinase when Tyr319 is phosphorylated (Schmidt et al., 2005), and the second patch forms the binding site for the CHMP4B subunits of the ESCRT-III complex (Kim et al., 2005 and see below). A strongly

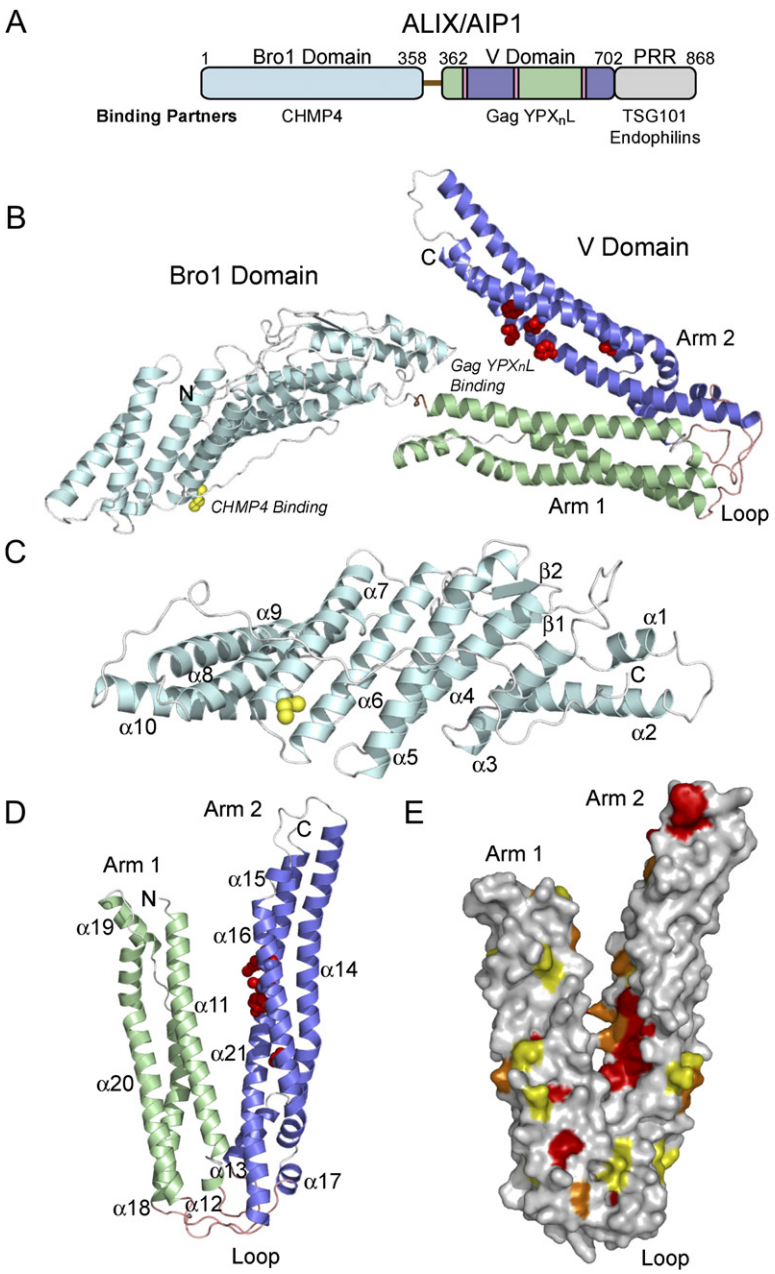

Figure 1. Structure of $ALIX_{Bro1-V}$

(A) shows domain structure of human ALIX. Sequences that compose the different elements are color coded here (and throughout) as follows: Bro1, turquoise; Bro1-V linker, brown; V-domain arm1, green; V-domain loop, salmon; V-domain arm2, blue; and Proline-rich region (PRR), gray.

(B) Ribbon representation of $ALIX_{Bro1-V}$ is shown. Residues implicated in CHMP4 binding (Ile212; yellow) or YPX_nL binding (Phe495, Val498, Ala509, Phe676, Leu680, and Ile683; red) are highlighted. The Bro1 and V domains are connected by a short hydrophobic linker ($_{359}VPV_{361}$). The limited set of interdomain hydrophobic packing interactions is made by Phe24 (α1, Bro1), Val359, Pro360, Val361, Val363 (α11, arm1, and V), and Leu585 (α19, arm1, and V).

(C) This ribbon diagram of $ALIX_{Bro1}$ shows the secondary-structure-labeling scheme. The view is from the underside of the orientation shown in (A).

(D) shows a ribbon diagram of $ALIX_V$ showing the secondary-structure-labeling scheme. As compared to (A), this orientation is rotated clockwise by ~60° relative to a line perpendicular to the plane of the paper.

(E) This surface rendering shows $ALIX_V$ sequence conservation. $ALIX_V$ sequences from seven divergent species were aligned using ESPript (Gouet et al., 1999); residues with scaled similarity scores are color coded as follows: 85–100 are red, 68–84 are orange, and 50–67 are yellow.

electropositive patch at one end of the yeast Bro1 domain is also basic in the human protein, albeit to a lesser extent.

The human and yeast Bro1 domains differ most at one end of the domain (right in Figure 1C), where N- and C-terminal elements differ in secondary structure and packing (Figure S2). Specifically, the C terminus of yeast Bro1p forms three consecutive helical segments that cross the concave side and then turn up into the domain, whereas the equivalent residues in the human protein (342–358) form an extended strand that traverses a similar path but terminates earlier. Thus, the C-terminal helix of the yeast protein packs between α3 and the α1–2 hairpin ($ALIX_{Bro1}$ numbering), whereas the human Bro1 C terminus is shifted by ~10 Å, and the first three helices of human $ALIX_{Bro1}$ collapse into a three-helix bundle (a maximal relative shift of ~12 Å). It appears possible that these distinct C-terminal conformations could alter the relative orientations of the Bro1 and V domains in the different proteins.

The Structure of the ALIX V Domain

Both arms of the ALIX V domain are composed of extended three-helix bundles, although a series of short breaks subdivide the major helices into 11 different segments (Figures 1D, S1, and S3). The topology of the V domain is notable in that the polypeptide chain crosses the arm1/arm2 "loop" region three times in the course of

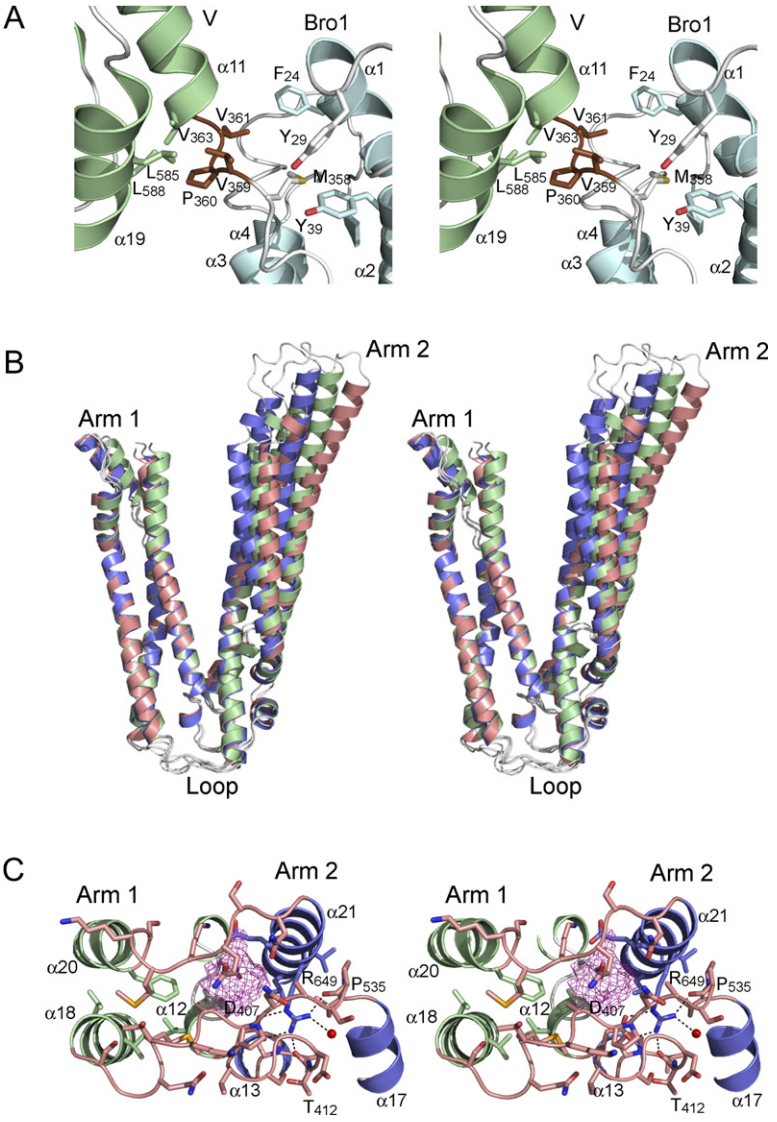

Figure 2. Interdomain Linkers and Conformational Flexibility of $ALIX_{Bro1-V}$

(A) Stereoview showing the linker between the Bro1 and V domains is shown. Secondary structures are color coded as in Figure 1B, and residues that contact the $_{359}VPV_{361}$ linker are shown explicitly.

(B) This stereoview illustrates conformational variability in different V-domain structures. The different trajectories of arm2 were visualized by superimposing only the arm1 regions from crystals of $ALIX_{Bro1-V}$ (salmon) and from the two different molecules in the $ALIX_V$ asymmetric unit (green and blue). The only other significant difference between the structures was in the position of Trp476 residue (α4/5 loop), which flips out of the core of arm2 in one of the two $ALIX_V$ structures to make a crystal contact.

(C) shows a stereoview illustrating the three-stranded loop region that connects the two arms of the V domain. Secondary structures are color coded as in Figure 1B. Side chains within the loop and adjacent residues are shown, and the stabilizing interactions of the Arg649 residue are shown explicitly. The purple cage denotes a pocket that appears to be occupied by a mix of ordered and disordered water molecules. The view is from the bottom of (B).

building the two helical bundles (Figure S3). Hence, the two arms are highly interconnected in primary sequence, and the entire V domain likely represents a single functional entity.

The two V-domain arms are primarily stabilized by hydrophobic side-chain-packing interactions that are based upon heptad repeats and that adopt canonical "knobs into holes" side-chain packing. This explains why the domain scored highly in coiled-coil prediction algorithms (Katoh et al., 2003; Odorizzi et al., 2003). In contrast, the three strands in the loops connecting arm1 and arm2 are stabilized almost exclusively by hydrophilic interactions, most of which are mediated by backbone atoms. An illustrative example is provided by the highly conserved Arg649 residue (α21, arm2), which forms a series of interactions that buttress the underside of the loop region; these include a buried salt bridge with Asp407 (α12/13 loop) and hydrogen-bonding interactions with a buried water molecule and with the backbone carbonyl oxygen atoms of Pro535 (α17/18 loop) and Thr412 (α12/13 loop). The loop region also encloses a hydrophilic interior cavity of ~67 $Å^3$ (purple in Figure 2C).

The V domain exhibits intrinsic conformational flexibility, as revealed by comparisons of the relative positions of the two arms in the different crystal structures. Isolated arm1 structures from the crystallographically independent models overlap well (rmsd = 1.4 Å), and the same is true for the arm2 structures, but overlapping on either arm causes the other to "fan out" into different positions. This is illustrated in Figure 2B for the case of overlap on arm1, where the relative arm2 displacements reach up to 10 Å at their distal ends. These global differences in the structures arise from small, cumulative changes in the interhelical packing interactions along both arms rather than from a dramatic reorganization of the loop region or elsewhere. Thus, the structures demonstrate that the V-domain arm

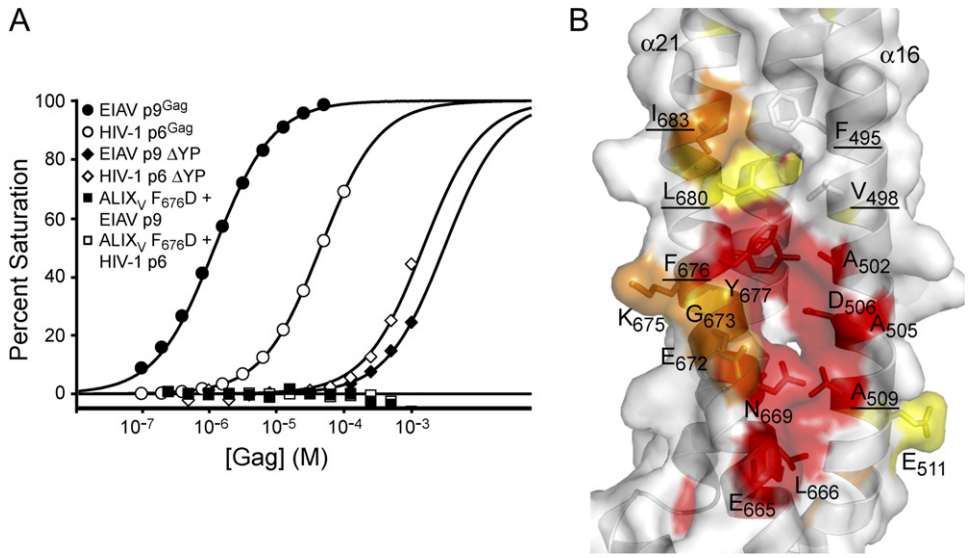

Figure 3. Identification of the YPX$_n$L-Binding Site on ALIX$_V$

(A) Biosensor binding isotherms for purified HIV-1 p6^{Gag} and EIAV p9^{Gag} constructs binding to immobilized ALIX$_V$ domain constructs are shown.

(B) YPX$_n$L-binding site on ALIX$_V$ arm2 is shown here as viewed from arm1. Residue conservation is color coded as in Figure 1E. Underlined residues were mutated and tested for YPX$_n$L-binding activity and/or for activity in the HIV-1 ΔPTAP rescue assay (see text).

positions can vary, although the biological significance of this observation remains to be elucidated.

The ALIX V Domain Binds HIV-1 p6^{Gag} and EIAV p9^{Gag} YPX$_n$L Late Domains

ALIX binds and facilitates budding of retroviral Gag proteins that contain YPX$_n$L late domains, but the interaction site is not yet known. We therefore performed biosensor binding experiments to map the YPX$_n$L-binding site and measure the binding affinities of the HIV-1 p6^{Gag} and EIAV p9^{Gag} proteins. As shown in Figure 3A, the immobilized ALIX V domain bound both HIV-1 p6^{Gag} and EIAV p9^{Gag}, with dissociation constants of 59 ± 15 μM and 1.2 ± 0.3 μM, respectively. In both cases, binding was specific for the YPX$_n$L late domain because YP to SR mutations (termed ΔYP; Strack et al., 2003) reduced binding affinities substantially (>15-fold). Very similar binding data were also obtained for the ALIX$_{Bro1\text{-}V}$ construct, which indicates that the Bro1 domain did not contribute to the binding interaction (Table S2).

Close inspection of the V-domain surface revealed a highly conserved hydrophobic groove on arm2 between helices 16 and 21, centered about Phe676, that was a strong candidate for the YPX$_n$L late-domain-binding site (Figures 1D, 1E, 3B, and S4). This site is exposed to solvent but is located near the base of the V, where the two arms are separated by only 5–10 Å. Phe676 sits at one end of a deep pocket (~10 Å) that is lined by a series of highly conserved residues (highlighted in red in Figure 3B). A shallower hydrophobic groove also extends ~7 Å above Phe676, although the residues that line this half of the site are less well conserved (Figures 3B, S1, and S4).

Mutational analyses confirmed that a series of conserved residues within the putative YPX$_n$L-binding site on arm2 were required for full-affinity HIV-1 p6^{Gag} and EIAV p9^{Gag} binding. As shown in Figure 3A, the Phe676Asp mutation abolished any detectable binding to either HIV-1 p6^{Gag} or EIAV p9^{Gag}, which represents a >1000-fold reduction in EIAV p9^{Gag} binding affinity. Mutations in two other binding-groove residues (Val498Asp and Ile683Asp) also reduced HIV-1 p6^{Gag} and EIAV p9^{Gag} binding affinities substantially (≥20 fold; see Table S2). These data indicate that retroviral Gag YPX$_n$L late domains bind the V domain of ALIX at a conserved site that spans the side and interior face of arm2.

Requirements for ALIX in EIAV and HIV-1 Release

Previous studies have indicated that ALIX can function in the release of both EIAV and HIV-1 (Chen et al., 2005; Martin-Serrano et al., 2003; Strack et al., 2003; von Schwedler et al., 2003). Importantly, however, EIAV p9^{Gag} contains a single known late domain (the $_{23}$YPDL$_{26}$-ALIX site), whereas HIV-1 p6^{Gag} contains two late domains: a $_{7}$PTAP$_{10}$-TSG101 site and a $_{36}$YPLASL$_{41}$-ALIX site. We therefore assessed the relative importance of ALIX for the release of both EIAV and HIV-1. As shown in Figure 4A, the release of virion-associated Gag-derived CA protein from HeLa cells expressing a wild-type EIAV vector was readily detected in western blot assays (lane 1, upper panel), but the ΔYP mutation in the p9^{Gag} ALIX-binding site reduced EIAV particle release 12-fold (compare lanes 1 and 2, panel 1). ALIX depletion similarly reduced the

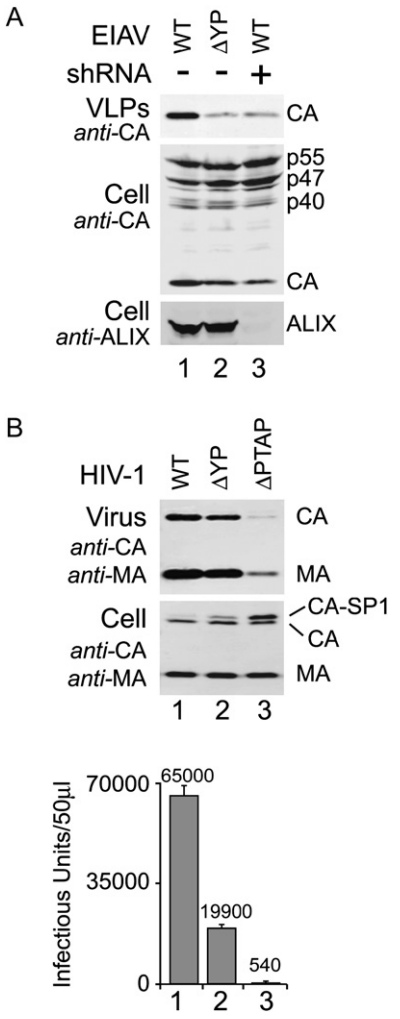

Figure 4. Requirement for ALIX in EIAV and HIV-1 Budding

(A) ALIX requirements for EIAV vector budding are shown as follows: lanes 1, wild-type (WT) EIAV vector expressed in wild-type HeLa cells (positive control); lanes 2, EIAV vector encoding a $_{23}SR_{24}$ mutation in the $_{23}YPDL_{26}$ late domain of $p9^{Gag}$ (ΔYP) expressed in wild-type HeLa cells; and lanes 3, wild-type EIAV vector expressed in cells depleted of ALIX using shRNA. Western blots are shown as follows: panel 1, virus-like particle (VLP) production (anti-CA antibody) reports the amount of successful budding and panel 2, cellular Gag protein levels (anti-CA antibody) control for expression. Note that CA corresponds to the processed central domain of Gag, p55 corresponds to full-length Gag protein, and p40 and p47 are intermediate Gag cleavage products. Cellular Gag levels were similar in all cases, although the processing was somewhat delayed in the ΔYP mutant and in the absence of ALIX. Panel 3 shows cellular ALIX levels (anti-ALIX antibody).

(B) The relative importance of ALIX and TSG101 binding for HIV-1 virus budding is shown. Lanes 1 show wild-type (WT) HIV-1 expressed in 293T cells (positive control), lanes 2 show HIV-1 encoding a $_{36}SR_{37}$ mutation in the $_{36}YPLASL_{41}$ late domain of $p6^{Gag}$ (ΔYP), and lanes 3 show wild-type HIV-1 encoding a $_{7}LIRL_{10}$ mutation in the $_{7}PTAP_{10}$ late domain of $p6^{Gag}$ (ΔPTAP). Western blots show virus production (panel 1) and cellular Gag protein levels (panel 2, anti-CA and anti-MA antibodies; MA is the processed N-terminal domain of Gag). Panel 3 shows viral titers measured in a single-cycle MAGIC assay (errors are standard deviations from three separate infectivity experiments). Note that cellular CA and MA levels were similar in all cases but that the CA-SP1-processing intermediate accumulated in the ΔYP and ΔPTAP constructs, which is a typical diagnostic of virus-budding inhibition.

release of wild-type EIAV 10-fold (compare lanes 1 and 3, upper panel). shRNA depletion of ALIX from HeLa cells was very efficient (lane 3, bottom panel), and EIAV Gag expression was not significantly affected by either the $p9^{Gag}$ ΔYP mutation or by ALIX depletion (middle panels). Gag processing was inhibited slightly, however, which is reminiscent of the Gag-processing delay observed upon inhibition of HIV-1 budding (Gottlinger et al., 1991). We therefore conclude that the $_{23}YPDL_{26}$-ALIX interaction plays a critical role in enhancing EIAV Gag release, which is in good agreement with previous studies (Martin-Serrano et al., 2003; Puffer et al., 1997; Strack et al., 2003).

The importance of ALIX for HIV-1 release was also tested by measuring the effect of the ΔYP mutation in the ALIX-binding site of HIV-1 $p6^{Gag}$. As shown in Figure 4B, this mutation reduced HIV-1 Gag release from 293T cells, as measured in both a western blot assay (compare lanes 1 and 2, panel 1) and by viral titers in a single-cycle MAGIC infectivity assay (lanes 1 and 2, panel 3). However, the reductions in release and infectivity were modest (~3-fold). In comparison, a mutation that blocked the $_{7}PTAP_{10}$-TSG101 interaction ($PTAP_{7\text{-}10}LIRL$, termed ΔPTAP) had a much more profound effect on HIV-1 release and reduced infectious titers more than 100-fold (Figure 4B, compare lanes 1 and 3). Neither late-domain mutation affected Gag protein expression, although both again delayed Gag processing, as evidenced by intracellular accumulation of the CA-SP1-processing intermediate, with the more profound effect again seen for the ΔPTAP mutation (Figure 4B, central panel). These experiments indicate that ALIX and TSG101 both enhance the release of wild-type HIV-1 from 293T cells but that the virus depends much more heavily upon the $_{7}PTAP_{10}$-TSG101 interaction. These studies again generally agree well with previous mutational analyses that utilized different HIV-1 constructs and cell types and were performed before the discovery of the $p6^{Gag}$ $_{36}YPLASL_{41}$-ALIX interaction (Demirov et al., 2002; Gottlinger et al., 1991; Huang et al., 1995).

ALIX Overexpression Rescues Release and Infectivity of HIV-1 ΔPTAP

The experiments described above demonstrate that the $p9^{Gag}$ $_{23}YPDL_{26}$-ALIX late-domain interaction plays a major role in facilitating EIAV release, yet the $p6^{Gag}$ $_{36}YPLASL_{41}$-ALIX interaction does not efficiently substitute for the $_{7}PTAP_{10}$-TSG101 interaction in supporting HIV-1 release. We hypothesized that this apparent discrepancy might reflect a reduced ability of HIV-1 to recruit ALIX owing to the lower affinity of the $p6^{Gag}$ YPX_nL-binding site. We therefore tested whether the inefficient release of the HIV-1 ΔPTAP virus from 293T cells could be "rescued" by increasing intracellular ALIX concentrations.

As shown in Figure 5, HIV-1 ΔPTAP release and infectivity were indeed stimulated very dramatically (~25-fold) by ALIX overexpression (Figure 5, panels 1 and 4, compare lanes 1 and 2). Hence, raising cellular ALIX levels could restore HIV-1 ΔPTAP infectivity to within ~20% of the wild-type virus. Importantly, ALIX overexpression did not alter intracellular Gag expression or processing (panel 2), which demonstrates that the enhancement occurred at late stages in particle assembly or budding. Control experiments also confirmed that the $p6^{Gag}{}_{36}$YPLASL$_{41}$-ALIX interaction was responsible for this enhancement because ALIX overexpression did not stimulate the release of an HIV-1 ΔPTAP virus that also lacked a functional ALIX-binding site (compare lanes 2 and 4). Indeed, the secondary ΔYP mutation actually reduced HIV-1 ΔPTAP release and infectivity by an additional 5-fold (compare lanes 3 and 4 to lane 1) presumably because the mutation also inhibited the ability of *endogenous* ALIX to mediate low-level release. These experiments demonstrate that ALIX can replace TSG101 in its role of supporting the efficient release of infectious HIV-1, provided ALIX is present at sufficient levels to overcome the modest affinity of the $_{36}$YPLASL$_{41}$-ALIX interaction.

ALIX YPX$_n$L-Binding Activity Is Required for Virus Release

The rescue of HIV-1 ΔPTAP release and infectivity upon ALIX overexpression provided a convenient assay for testing which ALIX activities were required for functional virus release. This assay was initially used to test whether ALIX mutations that inhibited YPX$_n$L binding in vitro also inhibited virus release through the ALIX pathway. As described previously, overexpression of wild-type ALIX enhanced the release and infectivity of HIV-1 ΔPTAP ~25-fold (Figure 6A, compare lanes 1 and 2). In contrast, ALIX proteins with point mutations that inhibited YPX$_n$L binding (Val498Asp, Phe676Asp, and Ile683Asp) failed to rescue HIV-1 ΔPTAP release or infectivity (compare lanes 2 and 3–5). These mutations did not affect ALIX expression or stability (panel 3), nor did they affect cellular Gag levels (panel 2). Similar data were obtained for a series of other mutations within the YPX$_n$L-binding site (Phe495Asp, Val509Asp, and Leu680Asp), whereas mutations in a second conserved hydrophobic patch located on arm1 (Leu401Asp, Ile405Asp, and Leu556Asp) did not diminish ALIX rescue significantly (<2-fold, data not shown). These data reinforce the idea that ALIX binds YPX$_n$L late domains within the site shown in Figure 2B and demonstrate that ALIX mutations that impair YPX$_n$L binding also inhibit virus release and infectivity.

ALIX Recruitment of CHMP4/ESCRT-III Is Required for HIV-1 ΔPTAP Release

In addition to binding YPX$_n$L late domains, ALIX also binds CHMP4/ESCRT-III proteins through the Bro1 domain, suggesting that ALIX may serve to connect retroviral Gag proteins to the ESCRT-III machinery (Katoh et al., 2003; Kim et al., 2005; Martin-Serrano et al., 2003; Odorizzi et al., 2003; Strack et al., 2003; von Schwedler et al., 2003). We therefore tested whether the interaction between ALIX and CHMP4A was required for virus budding. Previous work showed that mutations in an exposed hydrophobic patch on yeast Bro1p inhibited Snf7p (CHMP4) binding and prevented proper MVB sorting (Kim et al., 2005). We found that a mutation within the equivalent patch on human ALIX, Ile212Asp, similarly inhibited the ALIX$_{Bro1}$-CHMP4A interaction, as assayed in a GST pulldown experiment (Figure 6B). As expected, wild-type ALIX$_{Bro1}$ bound to a GST-CHMP4A fusion protein but not to GST alone (compare lanes 2 and 3). In contrast, the ALIX$_{Bro1,I212D}$ mutant did not bind GST-CHMP4A detectably (compare lanes 3 and 6).

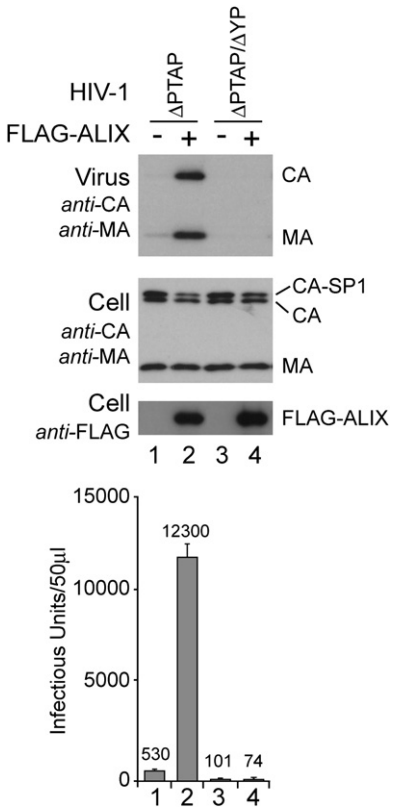

Figure 5. ALIX Overexpression Rescues HIV-1 ΔPTAP Release and Infectivity

Virus release, cellular Gag protein levels, exogenous ALIX expression, and viral infectivity are shown as analyzed by western blotting (panels 1–3) or MAGIC infectivity assays (panel 4). Lanes 1 show HIV-1 ΔPTAP cotransfected with an empty pCI-neo vector control, lanes 2 show HIV-1 ΔPTAP cotransfected with a vector expressing FLAG-ALIX, lanes 3 show HIV-1 ΔPTAP ΔYP cotransfected with an empty vector control, and lanes 4 show HIV-1 ΔPTAP ΔYP cotransfected with a vector expressing FLAG-ALIX. For reference, wild-type HIV-1 titers were typically ~65,000 IU/50 μl, and overexpression raised ALIX levels ~50-fold over endogenous protein levels as estimated by western blotting with anti-ALIX antibodies (not shown). Error bars in infectivity assays represent standard deviations of three separate infectivity experiments.

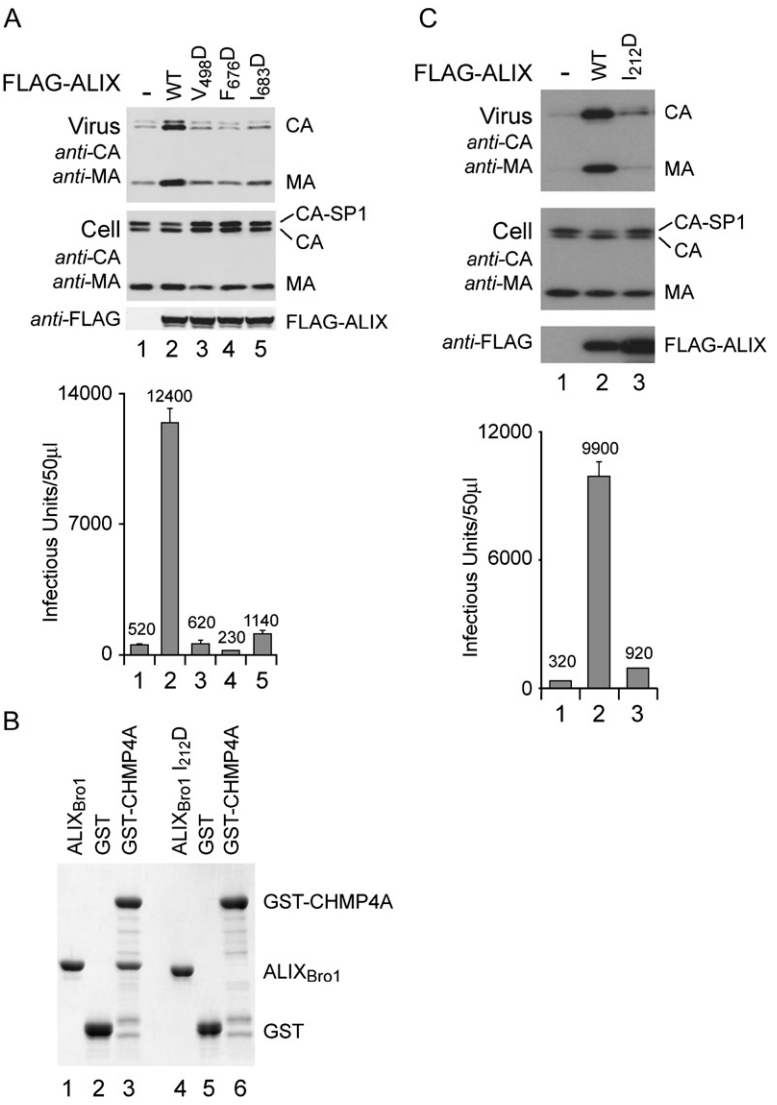

Figure 6. ALIX Mutants Lacking YPX_nL- and CHMP4-Binding Activities Do Not Support HIV-1 ΔPTAP Release and Infectivity

(A) HIV-1 ΔPTAP release and infectivity when coexpressed with an empty vector (–; lanes 1), with vectors expressing wild-type ALIX (lanes 2), or with ALIX mutants defective in YPX_nL binding (lanes 3–5) are shown. ALIX and Gag protein levels were analyzed by western blotting (panels 1–3), and infectious titers were analyzed using MAGIC assays (panel 4).

(B) This GST pulldown assay shows that the $ALIX_{Bro1}$ mutation Ile212Asp inhibits GST-CHMP4A binding. Binding experiments were performed with wild-type $ALIX_{Bro1}$ (lanes 1–3) and the $I_{212}D$ mutant (lanes 4–6). Lanes 1 and 4 show pure $ALIX_{Bro1}$ proteins (reference markers), lanes 2 and 4 show $ALIX_{Bro1}$ proteins binding to GST alone (negative controls), and lanes 3 and 6 show $ALIX_{Bro1}$ proteins binding to GST-CHMP4A.

(C) HIV-1 ΔPTAP release and infectivity are shown when coexpressed with an empty expression vector (–, lanes 1), with vectors expressing wild-type ALIX (lanes 2), or with the ALIX Ile212Asp mutant (lanes 3), which is defective in CHMP4A binding. In (A) and (C), HIV-1 ΔPTAP release, cellular Gag protein levels, exogenous ALIX expression, and viral infectivity were analyzed as described in Figure 4, with error bars representing standard deviations from three separate infectivity experiments.

We next tested whether the Ile212Asp mutation affected the ability of ALIX to rescue HIV-1 ΔPTAP infectivity. As shown in Figure 6C, the $ALIX_{I212D}$ mutant expressed well (panel 3, compare lanes 2 and 3) but failed to rescue HIV-1 ΔPTAP release or infectivity significantly (top and bottom panels, compare lanes 2 and 3). Hence, the Ile212Asp mutation strongly inhibited the ability of ALIX to support HIV-1 release, implying that one essential ALIX function in virus budding is to recruit CHMP4/ESCRT-III.

Other ALIX Functions in Virus Budding

The HIV-1 ΔPTAP rescue assay was also used to survey the functional importance of four other known ALIX properties: Tyr319 phosphorylation, TSG101 binding, endophilin binding, and interactions of the C-terminal PRR. ALIX mutants defective in each of these properties were generated and tested for their ability to rescue HIV-1 ΔPTAP release. In the first case, the ALIX Tyr319Phe mutation, which blocks phosphorylation and Src kinase binding (Schmidt et al., 2005), did not impair the rescue of HIV-1 ΔPTAP release and infectivity (Figure 7, lane 3). This result indicates that Src binding and phosphorylation do not play essential (or nonredundant) roles in ALIX virus-budding activity.

ALIX can also bind directly to the N-terminal UEV domain of TSG101 via a $_{717}PSAP_{720}$ motif located in the ALIX PRR (Martin-Serrano et al., 2003; Strack et al., 2003; von Schwedler et al., 2003). This interaction is of interest because it provides a potential mechanism for association of the two known late-domain-binding partners of HIV-1. As expected, mutation of the final proline in the $_{717}PSAP_{720}$ motif (Pro720Leu) eliminated TSG101 UEV binding entirely (Figure S5A). However, the $ALIX_{P720L}$ mutant fully rescued HIV-1 ΔPTAP release and infectivity (Figure 7, lane 4), which indicates that a functional TSG101-binding site was not required for ALIX to support virus budding. Indeed, we found that ALIX overexpression rescued HIV-1 ΔPTAP release even when TSG101 was

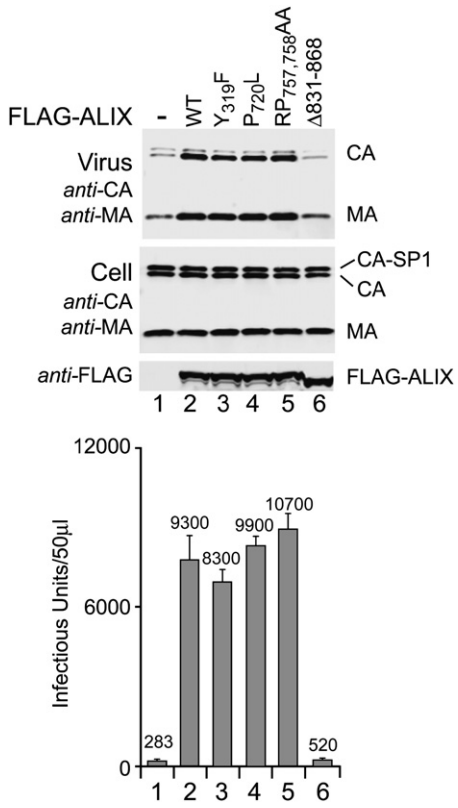

Figure 7. ALIX Requirements for HIV-1 ΔPTAP Release and Infectivity

HIV-1 ΔPTAP release and infectivity are shown when coexpressed with: an empty vector (−; lanes 1) with expression vectors for wild-type ALIX (lanes 2), with the ALIX $Y_{319}F$ mutant (lanes 3), which cannot be phosphorylated on residue 319, with the $ALIX_{P720L}$ mutant (lanes 4), which is defective in TSG101 binding, with the $ALIX_{RP757,758AA}$ mutant (lanes 5), which is defective in endophilin binding, or with the $ALIX_{\Delta 831-868}$ mutant (lanes 6), which lacks the final 38 residues in the PRR. HIV-1 ΔPTAP release, cellular Gag protein levels, exogenous ALIX expression, and viral infectivity were analyzed as described in Figure 4, with error bars representing standard deviations from three separate infectivity experiments.

depleted from cells (not shown), which indicates that the ALIX and TSG101 virus-budding pathways can function independently.

Endophilins represent another interesting class of ALIX-binding partners because endophilins can bind membranes and can drive (or sense) membrane curvature. Moreover, endophilin-2 binds and facilitates MLV Gag protein release (Wang et al., 2003). Endophilins bind the $_{755}PXRPPPP_{761}$ sequence within the ALIX PRR (Chatellard-Causse et al., 2002; Shibata et al., 2004). We employed yeast two-hybrid assays to confirm that the ALIX $RP_{757,758}AA$ mutation inhibited binding to both endophilin-1 and -2 (Figure S5B). Despite lacking endophilin-binding activity, however, the $ALIX_{RP757,758AA}$ mutant efficiently rescued HIV-1 ΔPTAP release and infectivity, which indicates that endophilin binding was also dispensable for the virus-budding function of ALIX (Figure 7, lane 5).

Finally, we tested the general importance of the ALIX PRR using several deletion mutants, the shortest of which removed just the final 38 ALIX residues ($ALIX_{\Delta 831-868}$). All of the C-terminal deletion mutants tested, including $ALIX_{\Delta 831-868}$, failed to rescue HIV ΔPTAP release and infectivity (lane 6) despite equivalent expression levels of the mutant and wild-type proteins (panel 3, compare lanes 2 and 6). We therefore conclude that ALIX PRR interaction(s) are required for late budding activity.

DISCUSSION

$ALIX_{Bro1-V}$ Structure

The elongated Bro1 domain extends from the first arm of the central V domain, which gives $ALIX_{Bro1-V}$ the shape of a "check mark." This distinctive conformation explains how Src kinase can bridge the N-terminal Bro1 domain and the distal PRR tail and how it may similarly bring other Bro1- and PRR-binding proteins into close proximity. The $ALIX_{Bro1-V}$ structure also suggests several ways in which conformational changes could function in the numerous biological roles ascribed to ALIX. Two types of domain motion are attractive possibilities: (1) variation in the relative orientation of the Bro1 and V domains, which appears possible given the limited number of contacts made by the interdomain linker (Figure 2A), and (2) variation in the trajectories of the two arms of the V domain, as implied by differences in the three different V-domain structures (Figure 2B).

In addition to the modest variation in arm orientation observed between crystal structures, we speculate that the V domain might function as a "molecular hinge," with the structures reported here corresponding to the closed conformation. This idea is consistent with the lack of hydrophobic packing interactions throughout the loop region of the V domain (Figure 2C). The hydrophilic loop-packing interactions that do exist are well defined and geometrically constrained, however, which indicates that if the loop functions as a hinge, then activation energy will be required to break these interactions and open the V. In principle, hinge opening could be driven by posttranslational modifications and/or ligand binding and might expose new binding sites and thereby provide an elegant mechanism for transmitting signals for complex assembly and disassembly. YPX_nL late domains are obvious candidates for triggering a possible hinge-opening motion because they bind near the base of the V at a site located nearly between the two arms.

YPX_nL Binding

We have mapped the YPX_nL-binding site to a conserved, hydrophobic groove on arm2 of the ALIX V domain and demonstrated that YPX_nL binding is required for ALIX-mediated budding of both HIV-1 and EIAV. ALIX binds nearly 60× more tightly to EIAV $p9^{Gag}$ than to HIV-1 $p6^{Gag}$, which is consistent with the idea that the EIAV $_{23}YPDL_{26}$ late

domain is an optimized ALIX-binding site (Vincent et al., 2003). This presumably reflects the fact that EIAV contains just a single known late domain and therefore relies heavily on ALIX to bud from cells. In contrast, the weaker HIV-1 $_{36}$YPLASL$_{41}$-ALIX late-domain interaction implies that suboptimal binding must confer a selective advantage when a functional TSG101-binding site is also present. This same trend can be seen in many different SIV strains, where the absence of a TSG101-binding site appears to correlate with the presence of an optimized ALIX-binding site (and vice versa; Bibollet-Ruche et al., 2004). Hence, viral late domains are not necessarily optimized for high-affinity binding, particularly when a virus employs multiple late domains.

We also found that ALIX can efficiently support the release and infectivity of an HIV-1 construct that lacks a TSG101-binding site, provided that the cellular ALIX levels are high enough to overcome the relatively weak binding affinity. Importantly, virus release via ALIX does not require TSG101, and vice versa. Similarly, TSG101 is not required for release of a Δp6 HIV-1 chimera that buds via a fused EIAV p9^{Gag} element (Martin-Serrano et al., 2003) nor for ALIX stimulation of murine leukemia virus budding (Segura-Morales et al., 2005). These observations all indicate that although TSG101 and ALIX can bind one another and function together in the MVB pathway, they represent independent routes out of the cell. The decisions as to which late domain(s) are employed by a particular virus, how many late domains are used, and the affinity of each binding site presumably reflect a complex optimization of the different possible exit routes from relevant host cell types.

Although the precise mechanistic role of the different cellular Class E proteins in enveloped virus budding is not yet clear, there is increasing evidence that viruses may be mimicking cellular interactions that allow membrane proteins to recruit the MVB machinery and be sorted into MVB vesicles, which ultimately leads to lysosomal degradation or release within extracellular exosomes. Interestingly, both the AP-2 adaptor complex and ALIX can bind a Tyr-based motif found in the cytoplasmic tail of the transferrin receptor (TR; although the motif does not match the YPX$_n$L consensus; Geminard et al., 2004). Vidal and colleagues have argued that the AP-2 interaction directs TR endocytosis, and the ALIX interaction may then direct the TR into exosomes that are released by maturing reticulocyte cells (Geminard et al., 2004). Both AP-2 and ALIX also bind the EIAV p9^{Gag} late domain and function in virus release (Chen et al., 2005), which suggests that EIAV may bud via the same pathway that sorts cellular TRs into reticulocyte-derived exosomes.

To date, the only well-documented example in which an ALIX-like protein binds a nonviral YPX$_n$L motif is for an ALIX homolog in *Aspergillus nidulans*, PalA, which binds tandem YPXL/I tetrapeptide repeats within PacC, a protein involved in sensing and responding to pH changes (Vincent et al., 2003). The YPXL/I motifs are required for pH-dependent proteolytic activation of PacC, although the precise role of PalA in this process is not clear. Other cellular binding partners for the ALIX V domain presumably exist, but the lack of a strong consensus sequence for the YPX$_n$L-like binding motifs complicates their identification.

Other Functional Requirements

Our studies also show that one essential function of ALIX in virus budding is to recruit the CHMP4/ESCRT-III complex. It has been challenging to establish a direct role for the ESCRT-III proteins in virus budding because human cells express 11 distinct, but related, ESCRT-III subunits, and it is therefore difficult to differentiate between nonessential versus redundant functions (e.g., see Langelier et al., 2006). Our work provides the most direct demonstration to date that ESCRT-III recruitment is required for virus budding and is consistent with previous studies showing that dominant-negative ESCRT-III constructs can block virus release (Martin-Serrano et al., 2003; Strack et al., 2003; von Schwedler et al., 2003) and that artificial Gag fusions that recruit ESCRT-III subunits can substitute for the $_{23}$YPDL$_{26}$ late domain in supporting EIAV p9^{Gag} release (Pineda-Molina et al., 2006). Hence, there is now increasing evidence that while enveloped RNA viruses can enter into the MVB pathway via many different binding partners, they ultimately require access to the ESCRT-III and VPS4-LIP5 complexes, which appear to be the functional machinery of MVB protein sorting/vesicle formation.

The PRR of ALIX also provides essential function(s) in virus budding. While the terminal 38 residues of ALIX could play a structural role, the high Pro and Gln content of this region (34% and 24%, respectively) makes it more likely that the polypeptide is inherently unstructured and can adopt an extended conformation that serves as the docking site for other cellular proteins. We have shown that endophilin and TSG101 binding to the PRR appear to be dispensable (or redundant) for viral budding. Determining the subset of PRR interactions that are essential for virus budding will likely shed light on the mechanistic requirements for protein sorting/vesicle formation and will further reveal how ALIX can serve as an adaptable, multidomain scaffold that links retroviral Gag proteins to essential cellular budding machinery.

EXPERIMENTAL PROCEDURES

Summary of Protein Expression, Purification, and Structure Determination

For protein-interaction studies, HIV-1 p6^{Gag} and EIAV p9^{Gag} were expressed as GST fusions in *E. coli* and purified by affinity chromatography and gel filtration chromatography (following protolytic removal of GST). ALIX$_{Bro1\text{-}V}$, ALIX$_{Bro1}$, and SeMet ALIX$_V$ were similarly expressed as GST or 6×-His N-terminal fusion proteins in *E. coli* and affinity purified for binding studies and crystallization. The 6x-His tag was left on crystallized ALIX$_{Bro1}$ but removed from ALIX$_{Bro1\text{-}V}$ and ALIX$_V$. The crystallized ALIX$_{Bro1\text{-}V}$ protein had a KK$_{268,269}$YY mutation. Structures were determined by SAD (ALIX$_V$) or molecular replacement (ALIX$_{Bro1}$ and ALIX$_{Bro1\text{-}V}$) and refined as summarized in Table S1. Full details of

plasmid construction, protein expression, crystallization, and structure determination are provided in the Supplemental Data.

Protein-Protein Interaction Experiments

Biosensor binding experiments were performed as described (Garrus et al., 2001) with purified HIV-1 $p6^{Gag}$, EIAV $p9^{Gag}$, and HIV-1 $TSG101_{UEV}$ proteins binding to immobilized GST-$ALIX_{Bro1\text{-}V}$, GST-$ALIX_{V}$, GST-$ALIX_{Bro1}$, and GST-$ALIX_{714–723}$ proteins. Assay conditions and binding affinities are provided in Table S2. GST pulldown experiments were performed as described (von Schwedler et al., 2003) using purified $ALIX_{Bro1}$ proteins binding to GST or GST-CHMP4A proteins captured from clarified *E. coli* lysates.

Assays for HIV-1 ΔPTAP Release and Infectivity

293T cells (~8×10^5 cells/well in 6-well plates) were transfected with 1 μg of HIV-1 ΔPTAP plasmid (Garrus et al., 2001) + 1 μg of ALIX expression vector per well (10 μl Lipofectamine 2000, Invitrogen). Cytoplasmic proteins and sucrose-pelleted virions were harvested 24 hr posttransfection, analyzed by western blotting, and quantified using an Odyssey imaging system (Li-COR, Inc.). Primary antibodies were rabbit anti-CA and rabbit anti-MA at 1:15,000. HIV-infectious titers were assayed in single-cycle MAGIC assays in P4 cells. Additional experimental details are provided in von Schwedler et al. (2003).

EIAV VLP Production and ALIX Silencing

HeLa M cells (~4×10^5 cells/well, 6-well plate) were transiently transfected (10 μl; FuGene6, Roche Applied Science) with 5 μg of wild-type or $p9^{Gag}$ ΔYP pEV53B EIAV vector (Olsen, 1998). EIAV virus-like particles were harvested 48 hr posttransfection, concentrated through 20% sucrose cushions, and analyzed by western blotting using affinity-purified EIAV anti-CA antibody (1:10,000). For ALIX-depletion experiments, an shRNA targeting human ALIX nucleotides 1765–1783 (Chen et al., 2005) was delivered using the FG12 lentiviral expression vector (Qin et al., 2003; 8 μg/ml polybrene, moi = 15) 24 hr prior to transfection with pEV53B.

Supplemental Data

Supplemental Data include Experimental Procedures, References, five figures, and two tables and can be found with this article online at http://www.cell.com/cgi/content/full/128/5/841/DC1/.

ACKNOWLEDGMENTS

We thank Michael Landesman for performing the yeast two-hybrid experiment shown in Figure S5 and Heidi Schubert, Andrew VanDemark, and Frank Whitby for helpful guidance in the crystallography. Operations of the National Synchrotron Light Source (NSLS) are supported by the Office of Basic Energy Sciences at the U.S. Department of Energy and by the National Institutes of Health (NIH). Data collection at the NSLS was funded by the National Center for Research Resources. This work was supported by NIH Grants GM066521 (C.P.H. and W.I.S.) and AI051174 (W.I.S.).

Received: November 13, 2006
Revised: December 22, 2006
Accepted: January 5, 2007
Published: March 8, 2007

REFERENCES

Alroy, I., Tuvia, S., Greener, T., Gordon, D., Barr, H.M., Taglicht, D., Mandil-Levin, R., Ben-Avraham, D., Konforty, D., Nir, A., et al. (2005). The trans-Golgi network-associated human ubiquitin-protein ligase POSH is essential for HIV type 1 production. Proc. Natl. Acad. Sci. USA *102*, 1478–1483.

Bibollet-Ruche, F., Bailes, E., Gao, F., Pourrut, X., Barlow, K.L., Clewley, J.P., Mwenda, J.M., Langat, D.K., Chege, G.K., McClure, H.M., et al. (2004). New simian immunodeficiency virus infecting De Brazza's monkeys (Cercopithecus neglectus): evidence for a cercopithecus monkey virus clade. J. Virol. *78*, 7748–7762.

Bieniasz, P.D. (2006). Late budding domains and host proteins in enveloped virus release. Virology *344*, 55–63.

Cabezas, A., Bache, K.G., Brech, A., and Stenmark, H. (2005). Alix regulates cortical actin and the spatial distribution of endosomes. J. Cell Sci. *118*, 2625–2635.

Chatellard-Causse, C., Blot, B., Cristina, N., Torch, S., Missotten, M., and Sadoul, R. (2002). Alix (ALG-2-interacting protein X), a protein involved in apoptosis, binds to endophilins and induces cytoplasmic vacuolization. J. Biol. Chem. *277*, 29108–29115.

Chen, C., Vincent, O., Jin, J., Weisz, O.A., and Montelaro, R.C. (2005). Functions of early (AP-2) and late (AIP1/ALIX) endocytic proteins in equine infectious anemia virus budding. J. Biol. Chem. *280*, 40474–40480.

Dejournett, R.E., Kobayashi, R., Pan, S., Wu, C., Etkin, L.D., Clark, R.B., Bogler, O., and Kuang, J. (2006). Phosphorylation of the proline-rich domain of XP95 modulates XP95 interaction with partner proteins. Biochem. J. *401*, 521–531.

Demirov, D.G., and Freed, E.O. (2004). Retrovirus budding. Virus Res. *106*, 87–102.

Demirov, D.G., Orenstein, J.M., and Freed, E.O. (2002). The late domain of human immunodeficiency virus type 1 p6 promotes virus release in a cell type-dependent manner. J. Virol. *76*, 105–117.

Gallop, J.L., and McMahon, H.T. (2005). BAR domains and membrane curvature: bringing your curves to the BAR. Biochem. Soc. Symp. *72*, 223–231.

Garrus, J.E., von Schwedler, U.K., Pornillos, O.W., Morham, S.G., Zavitz, K.H., Wang, H.E., Wettstein, D.A., Stray, K.M., Cote, M., Rich, R.L., et al. (2001). Tsg101 and the vacuolar protein sorting pathway are essential for HIV-1 budding. Cell *107*, 55–65.

Geminard, C., De Gassart, A., Blanc, L., and Vidal, M. (2004). Degradation of AP2 during reticulocyte maturation enhances binding of hsc70 and Alix to a common site on TFR for sorting into exosomes. Traffic *5*, 181–193.

Gottlinger, H.G., Dorfman, T., Sodroski, J.G., and Haseltine, W.A. (1991). Effect of mutations affecting the p6 gag protein on human immunodeficiency virus particle release. Proc. Natl. Acad. Sci. USA *88*, 3195–3199.

Gouet, P., Courcelle, E., Stuart, D.I., and Metoz, F. (1999). ESPript: analysis of multiple sequence alignments in PostScript. Bioinformatics *15*, 305–308.

Huang, M., Orenstein, J.M., Martin, M.A., and Freed, E.O. (1995). p6Gag is required for particle production from full-length human immunodeficiency virus type 1 molecular clones expressing protease. J. Virol. *69*, 6810–6818.

Hurley, J.H., and Emr, S.D. (2006). The ESCRT complexes: structure and mechanism of a membrane-trafficking network. Annu. Rev. Biophys. Biomol. Struct. *35*, 277–298.

Ichioka, F., Horii, M., Katoh, K., Terasawa, Y., Shibata, H., and Maki, M. (2005). Identification of Rab GTPase-activating protein-like protein (RabGAPLP) as a novel Alix/AIP1-interacting protein. Biosci. Biotechnol. Biochem. *69*, 861–865.

Katoh, K., Shibata, H., Suzuki, H., Nara, A., Ishidoh, K., Kominami, E., Yoshimori, T., and Maki, M. (2003). The ALG-2-interacting protein Alix associates with CHMP4b, a human homologue of yeast Snf7 that is involved in multivesicular body sorting. J. Biol. Chem. *278*, 39104–39113.

Kim, J., Sitaraman, S., Hierro, A., Beach, B.M., Odorizzi, G., and Hurley, J.H. (2005). Structural basis for endosomal targeting by the Bro1 domain. Dev. Cell *8*, 937–947.

Langelier, C., von Schwedler, U., Fisher, R.D., De Dominco, I., White, P.L., Hill, C.P., Kaplan, J., Ward, D., and Sundquist, W.I. (2006). Human ESCRT-II complex and its role in human immunodeficiency virus type 1 release. J. Virol. *80*, 9465–9480.

Luhtala, N., and Odorizzi, G. (2004). Bro1 coordinates deubiquitination in the multivesicular body pathway by recruiting Doa4 to endosomes. J. Cell Biol. *166*, 717–729.

Martin-Serrano, J., Zang, T., and Bieniasz, P.D. (2001). HIV-1 and Ebola virus encode small peptide motifs that recruit Tsg101 to sites of particle assembly to facilitate egress. Nat. Med. *7*, 1313–1319.

Martin-Serrano, J., Yaravoy, A., Perez-Caballero, D., and Bieniasz, P.D. (2003). Divergent retroviral late-budding domains recruit vacuolar protein sorting factors by using alternative adaptor proteins. Proc. Natl. Acad. Sci. USA *100*, 12414–12419.

Morita, E., and Sundquist, W.I. (2004). Retrovirus budding. Annu. Rev. Cell Dev. Biol. *20*, 395–425.

Odorizzi, G. (2006). The multiple personalities of Alix. J. Cell Sci. *119*, 3025–3032.

Odorizzi, G., Katzmann, D.J., Babst, M., Audhya, A., and Emr, S.D. (2003). Bro1 is an endosome-associated protein that functions in the MVB pathway in Saccharomyces cerevisiae. J. Cell Sci. *116*, 1893–1903.

Olsen, J.C. (1998). Gene transfer vectors derived from equine infectious anemia virus. Gene Ther. *5*, 1481–1487.

Pineda-Molina, E., Belrhali, H., Piefer, A.J., Akula, I., Bates, P., and Weissenhorn, W. (2006). The crystal structure of the C-terminal domain of Vps28 reveals a conserved surface required for Vps20 recruitment. Traffic *7*, 1007–1016.

Puffer, B.A., Parent, L.J., Wills, J.W., and Montelaro, R.C. (1997). Equine infectious anemia virus utilizes a YXXL motif within the late assembly domain of the Gag p9 protein. J. Virol. *71*, 6541–6546.

Qin, X.F., An, D.S., Chen, I.S., and Baltimore, D. (2003). Inhibiting HIV-1 infection in human T cells by lentiviral-mediated delivery of small interfering RNA against CCR5. Proc. Natl. Acad. Sci. USA *100*, 183–188.

Sadoul, R. (2006). Do Alix and ALG-2 really control endosomes for better or for worse? Biol. Cell *98*, 69–77.

Schmidt, M.H., Chen, B., Randazzo, L.M., and Bogler, O. (2003). SETA/CIN85/Ruk and its binding partner AIP1 associate with diverse cytoskeletal elements, including FAKs, and modulate cell adhesion. J. Cell Sci. *116*, 2845–2855.

Schmidt, M.H., Hoeller, D., Yu, J., Furnari, F.B., Cavenee, W.K., Dikic, I., and Bogler, O. (2004). Alix/AIP1 antagonizes epidermal growth factor receptor downregulation by the Cbl-SETA/CIN85 complex. Mol. Cell. Biol. *24*, 8981–8993.

Schmidt, M.H., Dikic, I., and Bogler, O. (2005). Src phosphorylation of Alix/AIP1 modulates its interaction with binding partners and antagonizes its activities. J. Biol. Chem. *280*, 3414–3425.

Segura-Morales, C., Pescia, C., Chatellard-Causse, C., Sadoul, R., Bertrand, E., and Basyuk, E. (2005). Tsg101 and Alix interact with murine leukemia virus Gag and cooperate with Nedd4 ubiquitin ligases during budding. J. Biol. Chem. *280*, 27004–27012.

Shibata, H., Yamada, K., Mizuno, T., Yorikawa, C., Takahashi, H., Satoh, H., Kitaura, Y., and Maki, M. (2004). The penta-EF-hand protein ALG-2 interacts with a region containing PxY repeats in Alix/AIP1, which is required for the subcellular punctate distribution of the amino-terminal truncation form of Alix/AIP1. J. Biochem. (Tokyo) *135*, 117–128.

Strack, B., Calistri, A., Craig, S., Popova, E., and Gottlinger, H.G. (2003). AIP1/ALIX is a binding partner for HIV-1 p6 and EIAV p9 functioning in virus budding. Cell *114*, 689–699.

Tsuda, M., Seong, K.H., and Aigaki, T. (2006). POSH, a scaffold protein for JNK signaling, binds to ALG-2 and ALIX in Drosophila. FEBS Lett. *580*, 3296–3300.

van der Goot, F.G., and Gruenberg, J. (2006). Intra-endosomal membrane traffic. Trends Cell Biol. *16*, 514–521.

VerPlank, L., Bouamr, F., LaGrassa, T.J., Agresta, B., Kikonyogo, A., Leis, J., and Carter, C.A. (2001). Tsg101, a homologue of ubiquitin-conjugating (E2) enzymes, binds the L domain in HIV type 1 Pr55Gag. Proc. Natl. Acad. Sci. USA *98*, 7724–7729.

Vincent, O., Rainbow, L., Tilburn, J., Arst, H.N., Jr., and Penalva, M.A. (2003). YPXL/I is a protein interaction motif recognized by aspergillus PalA and its human homologue, AIP1/Alix. Mol. Cell. Biol. *23*, 1647–1655.

von Schwedler, U.K., Stuchell, M., Muller, B., Ward, D.M., Chung, H.Y., Morita, E., Wang, H.E., Davis, T., He, G.P., Cimbora, D.M., et al. (2003). The protein network of HIV budding. Cell *114*, 701–713.

Wang, M.Q., Kim, W., Gao, G., Torrey, T.A., Morse, H.C., 3rd, De Camilli, P., and Goff, S.P. (2003). Endophilins interact with Moloney murine leukemia virus Gag and modulate virion production. J. Biol. *3*, 4.

Accession Numbers

Coordinates and data have been deposited into the Protein Data Bank (www.pdb.org; PDB codes 20EV, 20EW, and 20EX).

Cell, Volume *128*

Supplemental Data

Structural and Biochemical Studies of ALIX/AIP1 and Its Role in Retrovirus Budding

Robert D. Fisher, Hyo-Young Chung, Qianting Zhai, Howard Robinson, Wesley I. Sundquist, and Christopher P. Hill

SUPPLEMENTAL EXPERIMENTAL METHODS

Plasmid Construction

ALIX Protein Expression Constructs. ALIX coding sequences were amplified and subcloned from an EST clone (von Schwedler et al., 2003), and ALIX proteins were expressed as either 6x-His or GST N-terminal fusion proteins. For $ALIX_{Bro1\text{-}V}$ (residues 1-698) and $ALIX_{V}$ (residues 360-702), ALIX coding sequences were amplified with 5'*Nde*I and 3'*BamH*I restriction sites and inserted into the pET151/D-TOPO vector (Invitrogen) following the manufacturer's instructions. $ALIX_{Bro1}$ (residues 1-359) was cloned between 5'*Nde*I and 3'*BamH*I restriction sites in a modified pET16b vector (Novagen) designed to contain a TEV protease cleavage site following the 6x-His tag. GST-ALIX expression constructs were generated by inserting ALIX coding sequences between 5'*Nde*I and 3'*BamH*I restriction sites in a pGEX2T vector (GE Healthcare) modified to contain a TEV protease cleavage site and 5'*Nde*I and 3'*BamH*I/*Bgl*II restriction sites following the GST gene (pGEX2T-TEV).

HIV-1 $p6_{Gag}$ and EIAV $p9^{Gag}$ Expression Constructs. Genes encoding $HIV\text{-}1_{NL4\text{-}3}$ $p6^{Gag}$ and EIAV $p9^{Gag}$ were amplified from the proviral R9 and pEV53B plasmids (see below), with 5'*Nde*I and 3'*BamH*I restriction sites, to allow expression as GST fusion proteins

from a pGEX2T vector (GE Healthcare) modified to contain 5'*Nde*I and 3'*BamH*I cloning sites (Garrus et al., 2001; von Schwedler et al., 2003). ALIX point mutants were generated by the Quickchange (Stratagene) method, following the manufacturer's protocol.

GST-CHMP4A Expression Construct. The GST-CHMP4A expression construct used in GST pulldown experiments was described previously (von Schwedler et al., 2003). Note, however, that the CHMP4A and CHMP4B designations have been reversed from our previous publication to follow the convention of Katoh et al. (Katoh et al., 2003).

ALIX Mammalian Expression Vector. FLAG-tagged human ALIX DNA was amplified and an *Nde*I-*BamH*I fragment was subcloned into a pCI-neo vector (Promega) engineered to express the protein with an N-terminal FLAG epitope tag. ALIX mutants were constructed using the quick change method following manufacturer's instruction (Stratagene).

Virus Expression Constructs. HIV-1 proviral expression constructs were based on HIV-1_{NL4-3} R9ΔApa (Swingler et al., 1997) (a gift from Didier Trono, University of Lausanne). The HIV-1 $p6^{Gag}$ ΔPTAP construct has been described previously (Garrus et al., 2001). The HIV-1 $p6^{Gag}$ ΔYP was constructed using megaprimer mutagenesis to introduce the $_{36}YP_{37}$ to $_{36}SR_{37}$ mutation in $p6^{Gag}$ without altering the overlapping pol reading frame. The vector pEV53B (Olsen, 1998) (a gift from John Olsen, UNC Chapel Hill) was used to produce EIAV virus like particles, and the $_{23}YP_{24}$ to $_{23}SR_{24}$ mutation was introduced using the megaprimer method.

shRNA Lentiviral Vector for ALIX Depletion. An shRNA targeting human ALIX nucleotides 1765-1783 (Chen et al., 2005), was built into the FG12 lentiviral delivery

vector (Qin et al., 2003) (a gift from David Baltimore, Caltech). Lentiviral vectors packing this shRNA expression construct were produced in 293T cells by calcium phosphate co-transfection (8.1 µg FG12-ALIX shRNA, 8.1 µg pCMV∆R8.91 (Zufferey et al., 1997), and 2.7 µg pMD.G (Ory et al., 1996), 10 cm plate, ~4×10^6). Virus like particles were collected from the cell culture supernatants on the third day posttransfection and concentrated 200-fold by centrifugation through a 20% sucrose cushion.

Purification of Recombinant ALIX Proteins

$ALIX_{Bro1-V}$, $ALIX_{Bro1}$, and $ALIX_V$ were expressed as 6x-His N-terminal fusion proteins in BL21(DE3) Codon+ (RIL) *E. coli* grown in auto-induction media, ZYP-5052 (Studier, 2005), at 37°C for 5-6 hours with vigorous shaking in baffled flasks before moving to 23°C to grow to saturation within 16-18 hours. SeMet $ALIX_V$ was prepared by expression in PASM-5052 media (Studier, 2005). Subsequent purification steps were performed at 4°C unless noted. Cells were lysed with sonication and lysozyme treatment (2.5 mg/ml in 50 mM Tris pH 8.0, 300 mM NaCl, 10 mM imidazole). Clarified supernatant was applied to Ni^{2+}-NTA resin (Qiagen), washed with lysis buffer, and eluted with 25 mM Tris pH 8.0, 100 mM NaCl, 250 mM imidazole. For $ALIX_{Bro1}$, EDTA and DTT were added to 1 mM and the solution was diluted to 50 mM NaCl with ddH_2O. For $ALIX_{Bro1-V}$ and $ALIX_V$, the eluted protein was dialyzed against 25 mM Tris pH 8.0, 100 mM NaCl, 2 mM β-mercaptoethanol while incubating with TEV protease (~18 h, 23°C), and the processed protein was collected as flow-through from a second pass over Ni^{2+}-NTA resin and diluted to 50 mM NaCl. For all three constructs, protein

solutions were applied to a Q Sepharose FF column (GE Healthcare) and washed with 25 mM Tris pH 8.0, 50 mM NaCl, 1 mM DTT before eluting with a gradient to 1 M NaCl. Monomeric ALIX was separated from dimer ($ALIX_{Bro1-V}$ and $ALIX_V$ samples) and aggregated species by size exclusion chromatography in 10 mM Tris pH 8.0, 100 mM NaCl, 1 mM DTT: $ALIX_{Bro1-V}$ (Superdex 200, GE Healthcare), $ALIX_{Bro1}$ and $ALIX_V$ (Superdex 75, GE Healthcare). In the case of $ALIX_{Bro1-V}$ and $ALIX_V$, monomeric ALIX was the predominant species, while dimeric ALIX was present in a much lower percentage. Furthermore, rigorous equilibrium analytical ultracentrifugation showed that monomeric $ALIX_V$ remained monomeric and that there was no appreciable equilibrium between monomer and dimer species.

Purification of Recombinant HIV-1 $p6^{Gag}$ and EIAV $p9^{Gag}$

GST-$p6^{Gag}$ and GST-$p9^{Gag}$ were expressed and lysed (50 mM Tris pH 8.0, 300 mM NaCl, 1 mM DTT) as for ALIX constructs. Clarified lysate was applied to a Glutathione GSTPrep column (GE Healthcare), washed, and eluted with lysis buffer supplemented with 20 mM glutathione. Protein fractions were combined, made to 2.5 mM $CaCl_2$, and incubated with thrombin (Novagen). Free GST and uncut GST fusion protein was separated from free HIV-1 p6 or EIAV p9 by size exclusion chromatography (Superdex 75, GE Healthcare) in 20 mM NaPhosphate pH 7.2, 150 mM NaCl. Residual GST was removed by an additional pass through the Glutathione GSTPrep column.

ALIX Crystallization and Data Collection

All crystals were grown in sitting drops using protein concentrated to 10 mg/ml in the size exclusion chromatography solution. SeMet $ALIX_V$ crystals grew at 4°C with a reservoir of 0.16-0.20 M Magnesium formate and 14% PEG-3350, and a drop of 1-2 μL reservoir and 2 μL protein solution. $ALIX_{Bro1}$ and $ALIX_{Bro1\text{-}V}$ both crystallized best at 13°C in drops with equal (0.5 – 2.0 μL) volumes of protein and reservoir solution: $ALIX_{Bro1}$ — 0.1 M NaMES pH 6.5, 10% PEG-20,000. $ALIX_{Bro1\text{-}V}$ – 8-9% PEG 4000, 0.10-0.25 M ammonium acetate, 0.10-0.15 M Magnesium acetate, 0.05 M Hepes pH 7.0.

$ALIX_{Bro1}$ and $ALIX_V$ crystals were cryoprotected in solutions of reservoir made up with 20% glycerol ($ALIX_V$; 5% and 10% intermediate steps). $ALIX_{Bro1\text{-}V}$ cryoprotection used reservoir made up with 30% MPD, achieved in 5% increments. Crystals were suspended in a nylon loop, plunged into liquid nitrogen, and maintained at 100 K during data collection. Crystallographic statistics are given in Supplemental Table S1.

ALIX Structure Solution and Refinement

The $ALIX_V$ structure was determined by the SAD method. The top 8 Se sites located with SHELX (Schneider and Pape, 2004; Sheldrick and Schneider, 1997) were used in SOLVE/RESOLVE (Terwilliger, 2002) to estimate phases at 3.1 Å. Phases were further improved in SIGMAA (Read, 1986) by averaging estimates obtained from two crystals, and used with amplitudes of crystal 1 for map calculation. Initial polyalanine models were built for the two molecules in the asymmetric unit and used to guide averaging of the map separately over the regions of arm1 and arm2 using MAMA

(Kleywegt and Jones, 1999) and AVE (Jones, 1992). This improved map allowed fitting of the amino acid sequence.

The $ALIX_{Bro1}$ and $ALIX_{Bro1\text{-}V}$ structures were solved by molecular replacement using PHASER (McCoy et al., 2005). The search model for $ALIX_{Bro1}$ was a mixed poly-Ser/homology model based on the yeast Bro1 structure (pdb code 1ZB1) (Kim et al., 2005). Search models for $ALIX_{Bro1\text{-}V}$ were the refined structures of $ALIX_{Bro1}$ and the two arms of $ALIX_V$. Modelbuilding was with O (Jones et al., 1991) and COOT (Emsley and Cowtan, 2004). Structures were refined with CNS (Brunger et al., 1998) and in the final cycles using REFMAC5 with TLS refinement using TLSMD (Merritt and Painter, 2006; Painter and Merritt, 2006), and TLSANL (Howlin et al., 1993) in the CCP4 suite (Group, November 4. 1994). Figures of the structure were generated in PyMol (DeLano, 2002). Coordinates and data have been deposited in the Protein Data Bank, www.pdb.org (PDB code 2OEV, 2OEW, 2OEX).

SUPPLEMENTAL REFERENCES

Brunger, A.T., Adams, P.D., Clore, G.M., DeLano, W.L., Gros, P., Grosse-Kunstleve, R.W., Jiang, J.S., Kuszewski, J., Nilges, M., Pannu, N.S.*, et al.* (1998). Crystallography & NMR system: A new software suite for macromolecular structure determination. Acta Crystallogr. D Biol. Crystallogr. *54 (Pt 5)*, 905-921.

Chen, C., Vincent, O., Jin, J., Weisz, O.A., and Montelaro, R.C. (2005). Functions of early (AP-2) and late (AIP1/ALIX) endocytic proteins in equine infectious anemia virus budding. J. Biol. Chem. *280*, 40474-40480.

DeLano, W.L. (2002). The PyMOL Molecular Graphics System and Users Manual (San Carlos, CA, DeLano Scientific).

Emsley, P., and Cowtan, K. (2004). Coot: model-building tools for molecular graphics. Acta Crystallogr. D Biol. Crystallogr. *60*, 2126-2132.

Garrus, J.E., von Schwedler, U.K., Pornillos, O.W., Morham, S.G., Zavitz, K.H., Wang, H.E., Wettstein, D.A., Stray, K.M., Cote, M., Rich, R.L.*, et al.* (2001). Tsg101 and the vacuolar protein sorting pathway are essential for HIV-1 budding. Cell *107*, 55-65.

Group, C.C.P. (November 4. 1994). The CCP4 Suite:Programs for Protein Crystallography. Acta Crystallogr. D50, 760-763.

Holm, L., and Sander, C. (1998). Touring protein fold space with Dali/FSSP. Nucleic Acids Res. *26*, 316-319.

Howlin, B., Butler, S.A., Moss, D.S., Harris, G.W., and Driessen, H.P.C. (1993). TLSANL: TLS parameter analysis program for segmented anisotropic refinement of macromolecular structures. J. Appl. Crystallogr. *26*, 622-624.

Johnsson, B., Lofas, S., and Lindquist, G. (1991). Immobilization of proteins to a carboxymethyldextran-modified gold surface for biospecific interaction analysis in surface plasmon resonance sensors. Anal Biochem. *198*, 268-277.

Jones, T.A. (1992). A, yaap, asap, @#*? A set of averaging programs. In Molecular Replacement, E.J. Dodson, S. Gover, and W. Wolf, eds. (Warrington, SERC Daresbury Laboratory), pp. 91-105.

Jones, T.A., Zou, J.Y., Cowan, S.W., and Kjeldgaard (1991). Improved methods for binding protein models in electron density maps and the location of errors in these models. Acta Crystallogr. A *47 (Pt 2)*, 110-119.

Katoh, K., Shibata, H., Suzuki, H., Nara, A., Ishidoh, K., Kominami, E., Yoshimori, T., and Maki, M. (2003). The ALG-2-interacting protein ALIX associates with CHMP4b, a human homologue of yeast Snf7 that is involved in multivesicular body sorting. J. Biol. Chem.

Kim, J., Sitaraman, S., Hierro, A., Beach, B.M., Odorizzi, G., and Hurley, J.H. (2005). Structural basis for endosomal targeting by the Bro1 domain. Dev. Cell *8*, 937-947.

Kleywegt, G.J., and Jones, T.A. (1999). Software for handling macromolecular envelopes. Acta Crystallogr. D Biol. Crystallogr. *55*, 941-944.

Laskowski, R.A., MacArthur, M.W., Moss, D.S., and Thornton, J.M. (1993). PROCHECK: a program to check the stereochemical quality of protein structures. J. Appl. Crystallogr. *26*, 283-291.

McCoy, A.J., Grosse-Kunstleve, R.W., Storoni, L.C., and Read, R.J. (2005). Likelihood-enhanced fast translation functions. Acta Crystallogr. D Biol. Crystallogr. *61*, 458-464.

Merritt, E.A., and Painter, J. (2006). TLSMD web server for the generation of multi-group TLS models. J. Appl. Crystallogr. *39*.

Myszka, D.G. (1999). Improving biosensor analysis. J. Mol. Recognit. *12*, 279-284.

Olsen, J.C. (1998). Gene transfer vectors derived from equine infectious anemia virus. Gene Ther. *5*, 1481-1487.

Ory, D.S., Neugeboren, B.A., and Mulligan, R.C. (1996). A stable human-derived packaging cell line for production of high titer retrovirus/vesicular stomatitis virus G pseudotypes. Proc. Natl. Acad. USA *93*, 11400-11406.

Otwinowski, Z., and Minor, W. (1997). Processing of X-ray diffraction data collected in oscillation mode. Methods in Enzymol. *276*, 307-326.

Painter, J., and Merritt, E.A. (2006). Optimal description of a protein structure in terms of multiple groups undergoing TLS motion. Acta Crystallogr. D Biol. Crystallogr. *62*, 439-450.

Qin, X.F., An, D.S., Chen, I.S., and Baltimore, D. (2003). Inhibiting HIV-1 infection in human T cells by lentiviral-mediated delivery of small interfering RNA against CCR5. Proc. Natl. Acad. USA *100*, 183-188.

Read, R. (1986). Improved Fourier coefficients for maps using phases from partial structures with errors. Acta Crystallogr. A *42*, 140-149.

Schneider, T., and Pape, T. (2004). HKL2MAP: a graphical user interface for phasing with SHELX programs. J. Appl. Crystallogr. *37*, 843-844.

Sheldrick, G.M., and Schneider, T. (1997). SHELXL: High resolution refinement. Methods Enzymol. *277*, 319-343.

Studier, F.W. (2005). Protein production by auto-induction in high density shaking cultures. Protein Expr. Purif. *41*, 207-234.

Swingler, S., Gallay, P., Camaur, D., Song, J., Abo, A., and Trono, D. (1997). The Nef protein of human immunodeficiency virus type 1 enhances serine phosphorylation of the viral matrix. J. Virol. *71*, 4372-4377.

Terwilliger, T.C. (2002). Automated structure solution, density modification and model building. Acta Crystallogr. D Biol. Crystallogr. *58*, 1937-1940.

Thompson, J.D., Higgins, D.G., and Gibson, T.J. (1994). CLUSTAL W: improving the sensitivity of progressive multiple sequence alignment through sequence weighting, position-specific gap penalties and weight matrix choice. Nucleic Acids Res. *22*, 4673-4680.

von Schwedler, U.K., Stuchell, M., Muller, B., Ward, D.M., Chung, H.Y., Morita, E., Wang, H.E., Davis, T., He, G.P., Cimbora, D.M.*, et al.* (2003). The protein network of HIV budding. Cell *114*, 701-713.

Zufferey, R., Nagy, D., Mandel, R.J., Naldini, L., and Trono, D. (1997). Multiply attenuated lentiviral vector achieves efficient gene delivery in vivo. Nat. Biotechnol. *15*, 871-875.

Table S1. Data Collection and Refinement Statistics

	$ALIX_{Bro1-V}$ [a]	$ALIX_{Bro1}$ [a]	$ALIX_V$ [a]	
Data Collection [b]				
			Crystal 1	Crystal 2
Space Group	C2	C2	$P2_1$	$P2_1$
Cell Parameters (Å)	a = 144.0	a = 120.7	a = 63.9	a = 63.2
	b = 98.5	b = 63.2	b = 50.0	b = 49.8
	c = 72.2	c = 76.4	c = 130.2	c = 129.6
	ß = 105.6	ß = 122.1	ß = 101.1	ß = 101.2
Wavelength (Å)	1.1	1.54180	0.9792	0.9792
Resolution (Å)	30-3.30	30-2.55	50-2.60	50-2.60
Outer Shell (Å)	3.42-3.30	2.64-2.55	2.69-2.60	2.69-2.60
Number of reflections				
Total	727,803	178,235	1,048,903	1,677,930
Unique	14,236	15,487	23,601	22,229
Completeness (%)	94.6 (64.9)	96.5 (79.3)	92.4 (64.0)	89.8 (57.7)
R_{sym} (%)[b]	8.7 (28.8)	5.3 (24.0)	7.8 (20.4)	10.6 (29.7)
Mean I/s(I)	21.1 (3.5)	19.6 (3.6)	12.3 (3.6)	16.1 (3.2)
Refinement				
R factor/R_{free} (%)[c,d]	23.5/31.7	20.8/27.4	22.8/30.2	
Nonhydrogen atoms				
Total	5486	2910	5489	
Solvent	0	79	91	
RMSD from ideal geometry [e]				
Bond lengths (Å)	0.009	0.016	0.010	
Bond angles (º)	1.153	1.544	1.293	
Average B-factor ($Å^2$)	140.7	60.3	48.5	
Ramachandran plot, nonglycine residue in				
Most favorable region (%)	83.7	88.8	93.9	
Additional allowed region (%)	15.7	10.3	6.0	
Generous allowed region (%)	0.6	0.9	0.2	
Disallowed region (%)	0.0	0	0.0	

Values in parenthesis are for the highest resolution shell.

[a] The $ALIX_{Bro1-V}$ construct crystallized comprises ALIX residues Met1-Arg698 preceded by the vector sequence GIDPFTH. Of these, ALIX residues 2-698 are ordered in the refined model. The $ALIX_{Bro1}$ construct comprises ALIX residues Met1-Val359 preceded by MHHHHHHHHHHSGQNLYFQGH, and ALIX residues 1-358 are ordered. The $ALIX_V$ construct comprises ALIX residues Pro360-Arg702 preceded by GIDPFTHM, and ALIX residues 361-702 (molecule A) and 362-702 (molecule B) are ordered.

[b] Data were collected from single crystals at beamline X29 at the National Synchrotron Light Source, Brookhaven National Laboratory ($ALIX_V$ and $ALIX_{Bro1-V}$) or on a rotating anode source ($ALIX_{Bro1}$). Data were integrated and scaled with the HKL package (Otwinowski and Minor, 1997).

[b] $R_{sym} = (|(\sum I - \langle I \rangle)|)/(\sum I)$, where $\langle I \rangle$ is the average intensity of multiple measurements.

[c] R factor = $\sum_{hkl}||F_{obs}(hkl)|| - F_{calc}(hkl)||/\sum_{hkl}|F_{obs}(hkl)|$

[d] R_{free} = the crossvalidation R factor for 5% of reflections against which the model was not refined (7% for $ALIX_{Bro1-V}$).

[e] Geometry was analyzed in PROCHECK (Laskowski et al., 1993)

Table S2. ALIX Binding to HIV-1 $p6^{Gag}$ and EIAV $p9^{Gag}$

	Estimated Dissociation Constant (μM, 20°C)[a]				
	$ALIX_{Bro1\text{-}V}$ (WT)	$ALIX_V$ (WT)	$ALIX_V$ ($V_{498}D$)	$ALIX_V$ ($F_{676}D$)	$ALIX_V$ ($I_{683}D$)
HIV-1 $p6^{Gag}$	57 ± 21[b]	59 ± 15[b]	NB[c]	NB[c]	>1000[d]
HIV-1 $p6^{Gag}$ ΔYP	>1000[d]	>1000[d]	-	-	-
EIAV $p9^{Gag}$	1.5 ± 0.3[b]	1.2 ± 0.3[b]	18 ± 1	NB[b]	580 ± 20
EIAV $p9^{Gag}$ ΔYP	>1000[d]	>1000[d]	-	-	-

[a]Binding was measured using Biacore 2000 and 3000 optical biosensors (Biacore AB, Uppsala, Sweden) equipped with CM4 sensor chips derivatized with anti-GST antibodies through amine-coupling (Johnsson et al., 1991). GST (control) and GST-ALIX fusion proteins were captured from crude *E. coli* lysates to densities of 1000-1800 RU, and chip surfaces were over-coated with recombinant GST to minimize non-specific interactions. Purified wild-type and mutant HIV-1 $p6^{Gag}$ and EIAV $p9^{Gag}$ were diluted in running buffer (20 mM NaPhosphate, 150 mM NaCl, 0.2 mg/mL BSA, 0.005% P20, pH 7.2), and injected in duplicate from concentrations of 0 μM to 1000 μM. Affinity parameters were obtained by plotting the equilibrium responses against the analyte concentration and fitting to a simple 1:1 binding model (e.g., see Figure 3A)(Myszka, 1999).

[b]Average ± difference between 8 ($ALIX_{Bro1\text{-}V}$) or 6 ($ALIX_V$) independent measurements (errors in other measurements were estimated from statistical fits of the binding data).

[c]NB = No detectable binding.

[d]Weak binding was detectable, but could not be accurately quantified because half-maximal binding was not achieved.

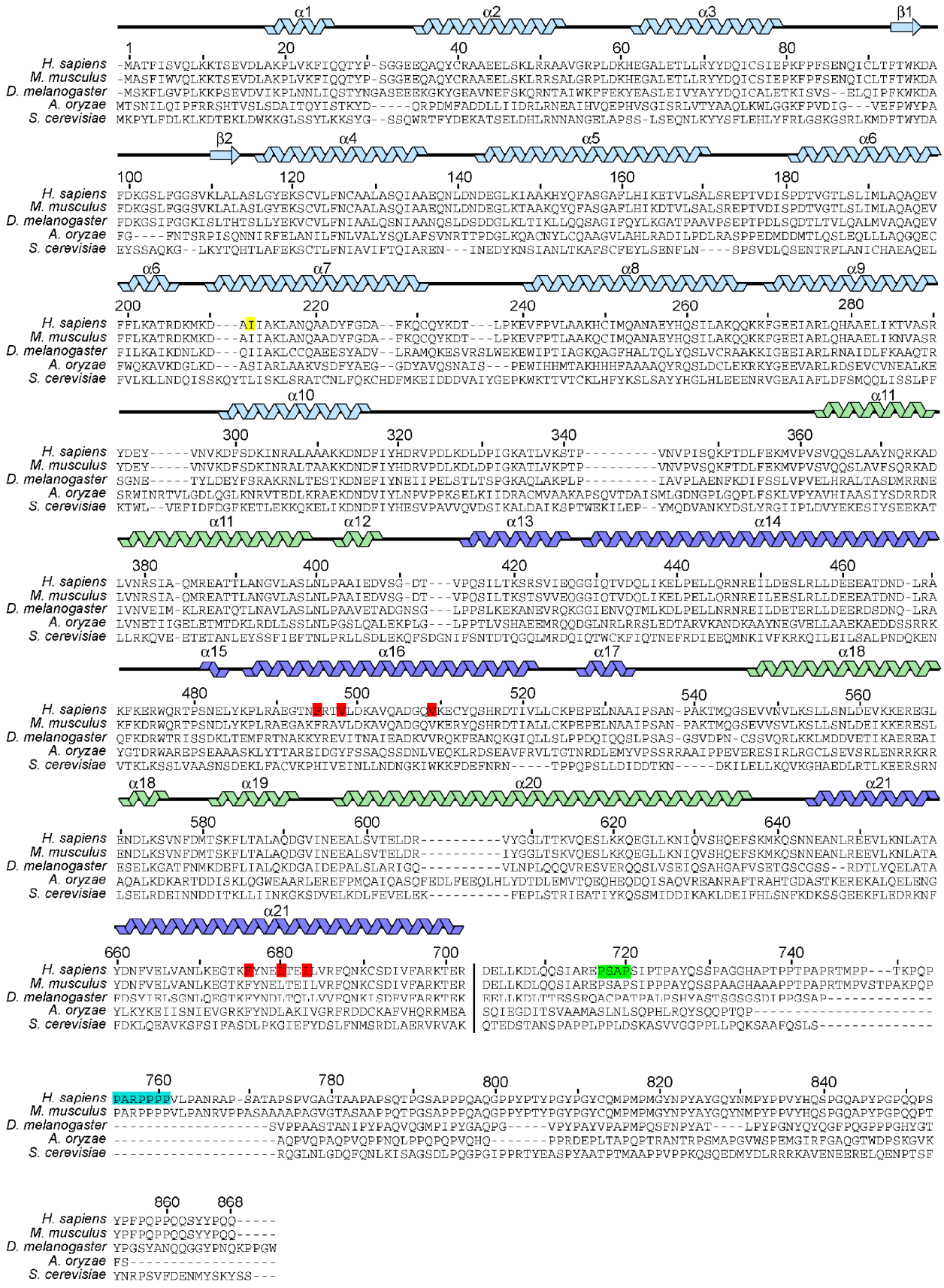
α1 α2 α3 β1
1 20 40 60 80
H. sapiens -MATFISVQLKKTSEVDLAKPLVKFIQQTYP-SGGEEQAQYCRAAEELSKLRRAAVGRPLDKHEGALETLLRYYDQICSIEPKFPFSENQICLTFTWKDA
M. musculus -MASFIWVQLKKTSEVDLAKPLVKFIQQTYP-SGGEEQAQYCRAAEELSKLRRSALGRPLDKHEGALETLLRYYDQICSIEPKFPFSENQICLTFTWKDA
D. melanogaster -MSKFLGVPLKKPSEVDVIKPLNNLIQSTYNGASEEEKGKYGEAVNEFSKQRNTAIWKFFEKYEASLEIVYAYYDQICALETKISVS--ELQIPFKWKDA
A. oryzae MTSNILQIPFRRRSHTVSLSDAITQYISTKYD-----QRPDMFADDLLIIDRLRNEAIHVQEPHVSGISRLVTYAAQLKWLGGKFPVDIG---VEFPWYPA
S. cerevisiae MKPYLFDLKLKDTEKLDWKKGLSSYLKKSYG--SSQWRTFYDEKATSELDHLRNNANGELAPSS-LSEQNLKYYSFLEHLYFRLGSKGSRLKMDFTWYDA
β2 α4 α5 α6
100 120 140 160 180
H. sapiens FDKGSLFGGSVKLALASLGYEKSCVLFNCAALASQIAAEQNLDNDEGLKIAAKHYQFASGAFLHIKETVLSALSREPTVDISPDTVGTLSLIMLAQAQEV
M. musculus FDKGSLFGGSVKLALASLGYEKSCVLFNCAALASQIAAEQNLDNDEGLKTAAKQYQFASGAFLHIKDTVLSALSREPTVDISPDTVGTLSLIMLAQAQEV
D. melanogaster FDKGSIFGGKISLTHTSLLYEKVCVLFNIAALQSNIAANQSLDSDDGLKLTIKLLQQSAGIFQYLKGATPAAVPSEPTPDLSQDTLTVLQALMVAQAQEV
A. oryzae FG----FNTSRPISQNNIRFELANILFNLVALYSQLAFSVNRTTPDGLKQACNYLCQAAGVLAHLRADILPDLRASPPEDMDDMTLQSLEQLLLAQGQEC
S. cerevisiae EYSSAQKG--LKYTQHTLAFEKSCTLFNIAVIFTQIAREN---INEDYKNSIANLTKAFSCFEYLSENFLN----SPSVDLQSENTRFLANICHAEAQEL
α6 α7 α8 α9
200 220 240 260 280
H. sapiens FFLKATRDKMKD---AIIAKLANQAADYFGDA--FKQCQYKDT---LPKEVFPVLAAKHCIMQANAEYHQSILAKQQKKFGEEIARLQHAAELIKTVASR
M. musculus FFLKATRDKMKD---AIIAKLANQAADYFGDA--FKQCQYKDT---LPKEVFPTLAAKQCIMQANAEYHQSILAKQQKKFGEEIARLQHAAELIKNVASR
D. melanogaster FILKAIKDNLKD---QIIAKLCCQAEESYADV--LRAMQKESVRSLWEKEWIPTIAGKQAGFHALTQLYQSLVCRAAKKIGEEIARLRNAIDLFKAAQTR
A. oryzae FWQKAVKDGLKD---ASIARLAAKVSDFYAEG--GDYAVQSNAIS---PEWIHHMTAKHHHFAAAAQYRQSLDCLEKRKYGEEVARLRDSEVCVNEALKE
S. cerevisiae FVLKLLNDQISSKQYTLISKLSRATCNLFQKCHDFMKEIDDDVAIYGEPKWKTTVTCKLHFYKSLSAYYHGLHLEEENRVGEAIAFLDFSMQQLISSLPF
α10 α11
300 320 340 360
H. sapiens YDEY-----VNVKDFSDKINRALAAAKKDNDFIYHDRVPDLKDLDPIGKATLVKSTP---------VNVPISQKFTDLFEKMVPVSVQQSLAAYNQRKAD
M. musculus YDEY-----VNVKDFSDKINRALTAAKKDNDFIYHDRVPDLKDLDPIGKATLVKPTP---------VNVPVSQKFTDLFEKMVPVSVQQSLAVFSQRKAD
D. melanogaster SGNE-----TYLDEYFSRAKRNLTESTKDNEFIYNEIIPELSTLTSPGKAQLAKPLP---------IAVPLAENFKDIFSSLVPVELHRALTASDMRRNE
A. oryzae SRWINRTVLGDLQGLKNRVTEDLKRAEKDNDVIYLNPVPPKSELKIIDRACMVAAKAPSQVTDAISMLGDNGPLGQPLFSKLVPYAVHIAASIYSDRRDR
S. cerevisiae KTWL--VEPIDFDGFKETLEKKQKELIKDNDFIYHESVPAVVQVDSIKALDAIKSPTWEKILEP--YMQDVANKYDSLYRGIIPLDVYEKESIYSEEKAT
α11 α12 α13 α14
380 400 420 440 460
H. sapiens LVNRSIA-QMREATTLANGVLASLNLPAAIEDVSG-DT---VPQSILTKSRSVIEQGGIQTVDQLIKELPELLQRNREILDESLRLLDEEEATDND-LRA
M. musculus LVNRSIA-QMREATTLANGVLASLNLPAAIEDVSG-DT---VPQSILTKSTSVVEQGGIQTVDQLIKELPELLQRNREILEESLRLLDEEEATDND-LRA
D. melanogaster IVNVEIM-KLREATQTLNAVLASLNLPAAVETADGNSG---LPPSLKEKANEVRQKGGIENVQTMLKDLPELLNRNREILDETERLLDEERDSDNQ-LRA
A. oryzae LVNETIIGELETMTDKLRDLLSSLNLPGSLQALEKPLG---LPPTLVSHAEEMRQQDGLNRLRRSLEDTARVKANDKAAYNEGVELLAAEKAEDDSSRRK
S. cerevisiae LLRKQVE-ETETANLEYSSFIEFTNLPRLLSDLEKQFSDGNIFSNTDTQGQLMRDQIQTWCKFIQTNEFRDIEEQMNKIVFKRKQILEILSALPNDQKEN
α15 α16 α17 α18
480 500 520 540 560
H. sapiens KFKERWQRTPSNELYKPLRAEGTNERTVLDKAVQADGQVKECYQSHRDTIVLLCKPEPELNAAIPSAN-PAKTMQGSEVVNVLKSLLSNLDEVKKEREGL
M. musculus KFKDRWQRTPSNDLYKPLRAEGAKFRAVLDKAVQADGQVKERYQSHRDTIALLCKPEPELNAAIPSAN-PAKTMQGSEVVSVLKSLLSNLDEIKKERESL
D. melanogaster QFKDRWTRISSDKLTEMFRTNAKKYREVITNAIEADKVVRQKFEANQKGIQLLSLPPDQIQQSLPSAS-GSVDPN-CSSVQRLKKLMDDVETIKAEREAI
A. oryzae YGTDRWAREPSEAAASKLYTTAREIDGYFSSAQSSDNLVEQKLRDSEAVFRVLTGTNRDLEMYVPSSRRAAIPPEVERESIRLRGCLSEVSRLENRRKRR
S. cerevisiae VTKLKSSLVAASNSDEKLFACVKPHIVEINLLNDNGKIWKKFDEFNRN-----TPPQPSLLDIDDTKN-----DKILELLKQVKGHAEDLRTLKEERSRN
α18 α19 α20 α21
580 600 620 640
H. sapiens ENDLKSVNFDMTSKFLTALAQDGVINEEALSVTELDR----------VYGGLTTKVQESLKKQEGLLKNIQVSHQEFSKMKQSNNEANLREEVLKNLATA
M. musculus ENDLKSVNFDMTSKFLTALAQDGVINEEALSVTELDR----------IYGGLTSKVQESLKKQEGLLKNIQVSHQEFSKMKQSNNEANLREEVLKNLATA
D. melanogaster ESELKGATFNMKDEFLIALQKDGAIDEPALSLARIGQ----------VLNPLQQQVRESVERQQSLVSEIQSAHGAFVSETGSCGSS--RDTLYQELATA
A. oryzae AQALKDKARTDDISKLQGWEAARLEREFPMQAIQASQFEDLFEEQLHLYDTDLEMVTQEQHEQDQISAQVREANRAFTRAHTGDASTKEREKALQELENG
S. cerevisiae LSELRDEINNDDITKLLIINKGKSDVELKDLFEVELEK----------FEPLSTRIEATIYKQSSMIDDIKAKLDEIFHLSNFKDKSSGEEKFLEDRKNF
α21
660 680 700 720 740
H. sapiens YDNFVELVANLKEGTKEYNELTELLVRFQNKCSDIVFARKTER DELLKDLQQSIAREPSAPSIPTPAYQSSPAGGHAPTPPTPAPRTMPP---TKPQP
M. musculus YDNFVELVANLKEGTKFYNELTEILVRFQNKCSDIVFARKTER DELLKDLQQSIAREPSAPSIPPPAYQSSPAAGHAAAPPTPAPRTMPVSTPAKPQP
D. melanogaster FDSYIRLSGNLQEGTKFYNDLTQLLVVFQNKISDFVFARKTEK ERLLKDLTTESSRQACPATPALPSHYASTSGSGSDIPPGSAP----------
A. oryzae YLKYKEIISNIEVGRKFYNDLAKIVGRFRDDCKAFVHQRRMEA SQIEGDITSVAAMASLNLSQPHLRQYSQQPTQP----------
S. cerevisiae FDKLQEAVKSFSIFASDLPKGIEFYDSLFNMSRDLAERVRVAK QTEDSTANSPAPPLPPLDSKASVVGGPPLLPQKSAAFQSLS----------
760 780 800 820 840
H. sapiens PARPPPPVLPANRAP-SATAPSPVGAGTAAPAPSQTPGSAPPPQAQGPPYPTYPGYPGYCQMPMPMGYNPYAYGQYNMPYPPVYHQSPGQAPYPGPQQPS
M. musculus PARPPPPVLPANRVPPASAAAAPAGVGTASAAPPQTPGSAPPPQAQGPPYPTYPGYPGYCQMPMPMGYNPYAYGQYNMPYPPVYHQSPGQAPYPGPQQPT
D. melanogaster ----------SVPPAASTANIPYPAQVQGMPIPYGAQPG-----VPYPAYVPAPMPQSFNPYAT----LPYPGNYQYQGFPQGPPPGHYGT
A. oryzae ----------AQPVQPAQPVQPPNQLPPQPQPVQHQ-------PPRDEPLTAPQPTRANTRPSMAPGVWSPEMGIRFGAQGTWDPSKGVK
S. cerevisiae ----------RQGLNLGDQFQNLKISAGSDLPQGPGIPPRTYEASPYAATPTMAAPPVPPKQSQEDMYDLRRRKAVENEERELQENPTSF
860 868
H. sapiens YPFPQPPQQSYYPQQ-----
M. musculus YPFPQPPQQSYYPQQ-----
D. melanogaster YPGSYANQQGGYPNQKPPGW
A. oryzae FS----------
S. cerevisiae YNRPSVFDENMYSKYSS---

Figure S1. Sequence Alignments, Secondary Structure, and Topology of Human $ALIX_{Bro1-V}$.

Sequence alignments of Bro1/ALIX proteins from five representative species, chosen because they are the most highly studied ALIX/Bro1 proteins. The secondary structure of human $ALIX_{Bro1-V}$ is shown above, together with the numbering scheme. The color coding is the same as in Fig. 1B, with the TSG101 binding site shown in lime green and the Endophilin binding site shown in turquoise. Sequence alignments were performed using the ClustalW server www.ebi.ac.uk/clustalw (Thompson et al., 1994), and match structure-based alignments for the Bro1 domain.

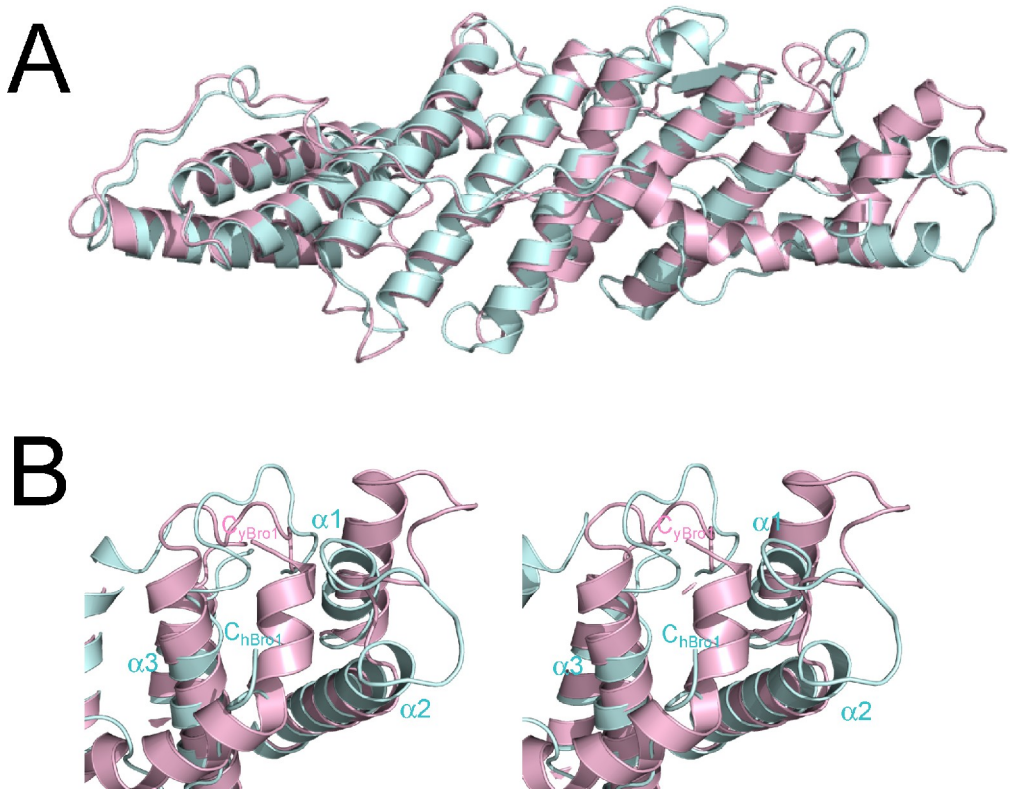

Figure S2. Comparison of the Human and Yeast Bro1 Domains.

(A) Superposition of human $ALIX_{Bro1}$ (turquoise) and yeast $Bro1_{Bro1}$ (magenta). Alignments were performed using the DALI server: http://www.ebi.ac.uk/dali (Holm and Sander, 1998).

(B) Stereoview showing a closeup view of the region with the greatest divergence between human $ALIX_{Bro1}$ (turquoise) and yeast $Bro1_{Bro1}$ (magenta). The region corresponds to the right edge of the image in (A). Helices a1-3 in human $ALIX_{Bro1}$ are labeled, as are the C-termini of human $ALIX_{Bro1}$ (C_{hBro1}) and yeast $Bro1_{Bro1}$ (C_{yBro1}).

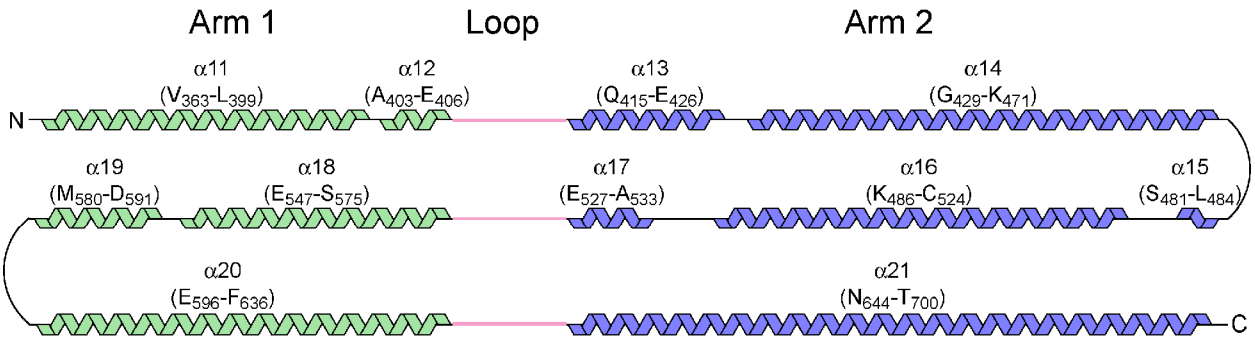

Figure S3. Topology of the ALIX$_V$ domain.

The figure illustrates how the polypeptide strand crosses the arm1/arm2 loop three times in the course of building the V domain. Color coding and numbering schemes are the same as in Fig. 1D.

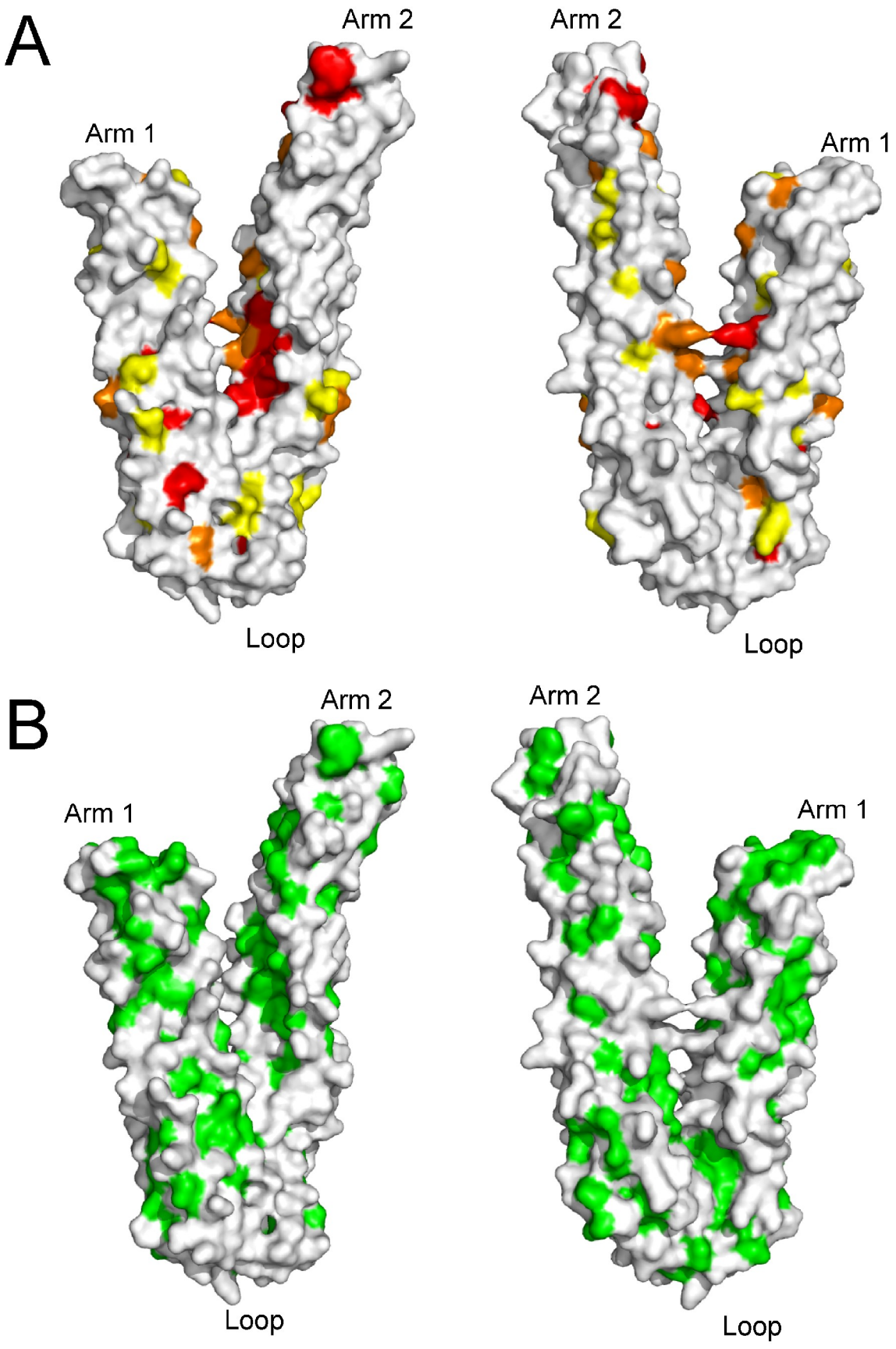
A
Arm 2
Arm 1
Loop
Arm 2
Arm 1
Loop
B
Arm 2
Arm 1
Loop
Arm 2
Arm 1
Loop

Figure S4. $ALIX_V$ Surface Conservation and Hydrophobicity

(A) Surface representation of $AlilX_V$ highlighting amino acid conservation. Coloring and orientation of the left molecule are the same as in Fig. 1E. The right molecule is the view from the "back" of the left. The nine species used in the alignment to define conservation are: *Homo sapiens* (Human), *Mus musculus* (Mouse), *Gallus gallus* (Chicken), *Xenopus laevis* (African clawed frog), *Drosophila melanogaster* (Fruit fly), *Caenorhabditis elegans*, *Dictyostelium discoideum* (Slime mold), *Arabidopsis thaliana* (Mouse-ear cress), and *Aspergillus oryzae*.

(B) Surface representation of $ALIX_V$ with surface residues colored by residue type. Hydrophobic residues are colored green, polar blue, and acidic/basic residues white. The molecule orientations are the same as in (A), except that the left molecule has been slightly rotated around the vertical axis to view the YPX_nL binding site on Arm2.

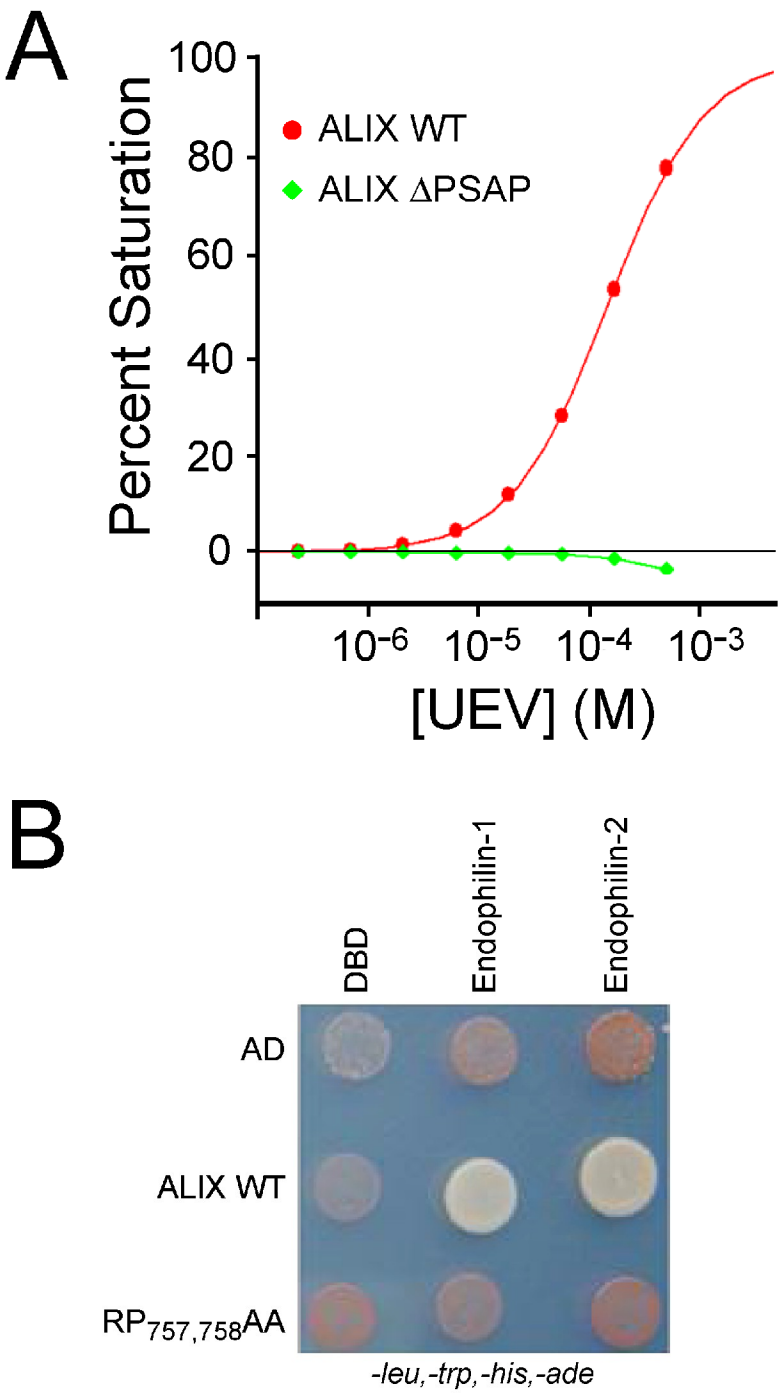

Figure S5. Characterization of ALIX Mutations that Block Endophilin and TSG101 Binding

(A) Biosensor binding isotherms showing that the TSG101 UEV domain binds a GST fusion construct spanning the wild type ALIX $_{717}$PSAP$_{720}$ motif (GST-ALIX$_{714-723}$,

K_d=146±1 μM), and that the Pro720Leu mutation (GST-$ALIX_{714\text{-}723,\ P720L}$) eliminated binding.

(B) Yeast two hybrid assay showing that human ALIX binds endophilins-1 and -2, and that the interactions are inhibited by the ALIX $RP_{757,758}$AA mutation. Directed yeast two hybrid assays were performed using the Matchmaker GAL4 Yeast Two Hybrid 3 system (Clontech). AH-109 *Saccharomyces cerevisiae* were co-transformed with pGADT7 or pGBKT7 cloning vectors (Clontech) containing inserts encoding wild type (WT) and mutant human ALIX (Activation Domain fusions, AD) and endophilins-1 and -2 (DNA Binding Domain fusions, DBD). Transformed yeast colonies were grown for three days at 30 °C on YPD plates with -Leu, -Trp selection. 10-100 colonies were pooled, resuspended in a liquid culture of SB (-Leu, -Trp), selected on SB (-Leu, -Trp, -Ade, -His) plates, and allowed to grow for 3 days. Growth on -Leu,-Trp,-His,-Ade media reflects positive binding interactions between ALIX and the endophilins, whereas failure to grow reflects a lack binding activity ($ALIX_{RP757,758AA}$ mutants and negative controls).